The specificity of pectate lyase VdPelB from Verticilium dahliae is highlighted by structural, dynamical and biochemical characterizations

Josip Safran, Vanessa Ung, Julie Bouckaert, Olivier Habrylo, Roland Molinié, Jean-Xavier Fontaine, Adrien Lemaire, Aline Voxeur, Serge Pilard, Corinne Pau-Roblot, et al.

International Journal of Biological Macromolecules

The specificity of pectate lyase VdPelB from Verticilium dahliae is highlighted by structural, dynamical and biochemical characterizations
### --Manuscript Draft--

Corresponding Author:	Fabien Sénéchal, Ph.D UMR1158: Transfrontaliere BioEcoAgro Amiens, FRANCE
First Author:	Josip Safran, Ph.D
Order of Authors:	Josip Safran, Ph.D
	Vanessa Ung
	Julie Bouckaert, Ph.D
	Olivier Habrylo, Ph.D
	Roland Molinié, Ph.D
	Jean-Xavier Fontaine, Ph.D
	Adrien Lemaire
	Aline Voxeur, Ph.D
	Serge Pilard, Ph.D
	Corinne Pau-Roblot, Ph.D
	Davide Mercadante, Ph.D
	Jérôme Pelloux, Pr.
	Fabien Sénéchal, Ph.D

Abstract:	Pectins, complex polysaccharides and major components of the plant primary cell wall, can be degraded by pectate lyases (PLs). PLs cleave glycosidic bonds of homogalacturonans (HG), the main pectic domain, by β-elimination, releasing unsaturated oligogalacturonides (OGs). To understand the catalytic mechanism and structure/function of these enzymes, we characterized VdPelB from Verticillium dahliae. We first solved the crystal structure of VdPelB at 1.2Å resolution showing that it is a right-handed parallel β-helix structure. Molecular dynamics (MD) simulations further highlighted the dynamics of the enzyme in complex with substrates that vary in their degree of methylesterification, identifying amino acids involved in substrate binding and cleavage of non-methylesterified pectins. We then biochemically characterized wild type and mutated forms of VdPelB. Pectate lyase VdPelB was most active on non-methylesterified pectins, at pH8.0 in presence of Ca2+ ions. The VdPelB-G125R mutant was most active at pH9.0 and showed higher relative activity compared to native enzyme. The OGs released by VdPelB differed to that of previously characterized PLs, showing its peculiar specificity in relation to its structure. OGs released from Verticillium-partially tolerant and sensitive flax cultivars differed which could facilitate the identification VdPelB-mediated elicitors of defence responses.

	Suzanna Saez-Aguayo Andrés Bello University susana.saez@unab.cl
Opposed Reviewers:	
Response to Reviewers:	

Highlights

- First crystallographic structure of Verticillium pectate lyase.
- Identification of key amino-acids for the activity
- Biochemical characterization of the enzyme and LC-MS/MS analysis of the oligogalacturonides (OG) produced
- Susceptible or partially resistant flax cultivars differ in OGs produced

Graphical abstract

PRIMARY CELL WALL

Homogalacturonan
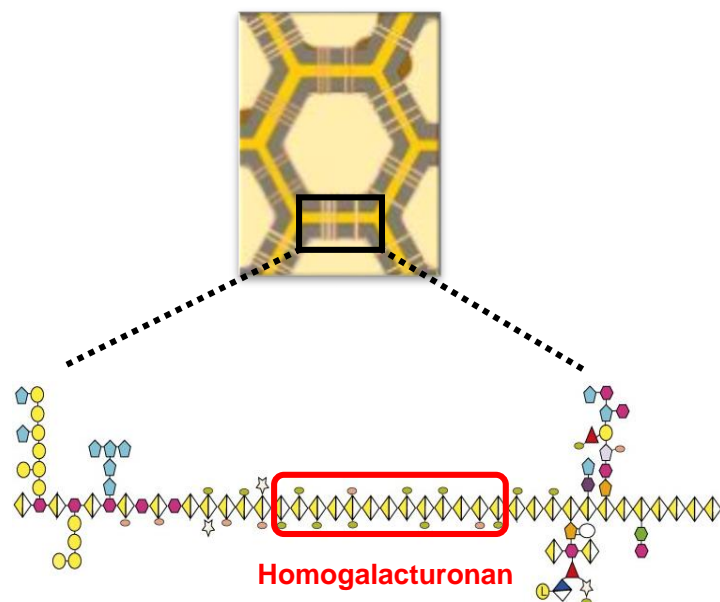
Pectate lyase like (PLLs) degrading enzymes
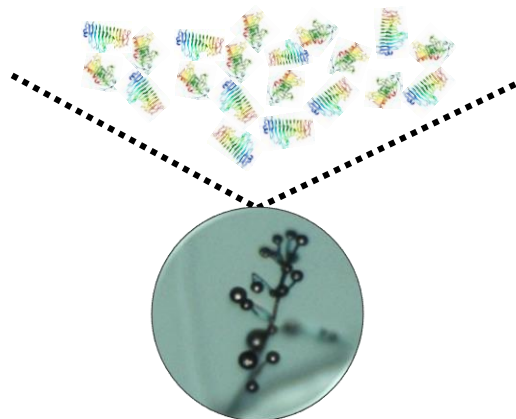
VERTICILLIUM DAHLIAE

VdPelB CRYSTAL STRUCTURE

BIOCHEMICAL CHARACTERIZATION

VdPelB-N
VdPelB-G125R
VdPelB-T157K

Relative activity (%)

pH5 pH6 pH7 pH7 pH8 pH9 pH10

NaP   Tris-HCl

MD SIMULATIONS

VdPelB substrate dynamics

-5   -5

+1   +1

+5   +5

RMSF analysis

Non-reducing end   Active Site   Reducing end

Mean RMSF (Å)

-5 -4 -3 -2 -1 +1 +2 +3 +4 +5
Monosaccharide subsite position

Nonmethyesterified sugar   Methyesterified sugar
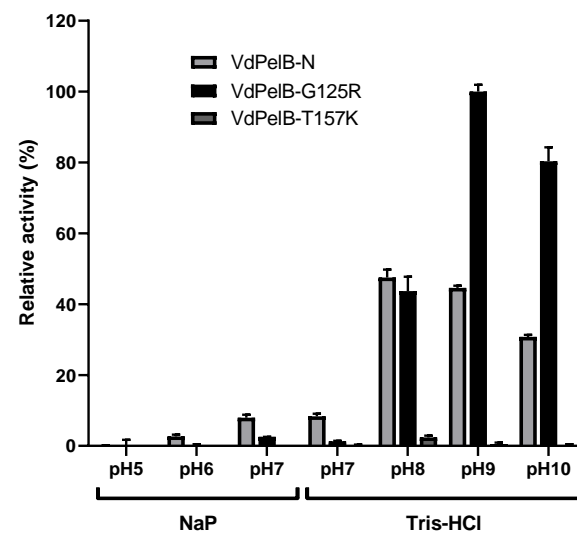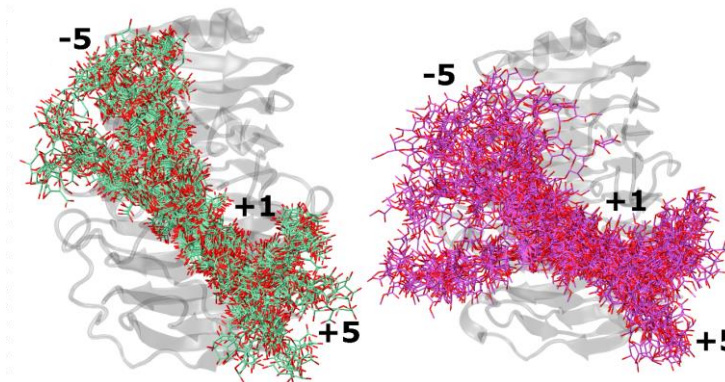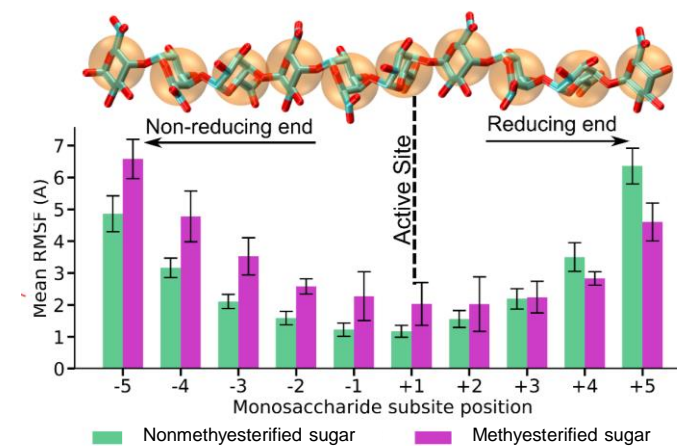
Declaration of interests

☐The authors declare that they have no known competing financial interests or personal relationships that could have appeared to influence the work reported in this paper.

☒The authors declare the following financial interests/personal relationships which may be considered as potential competing interests:

Abstract

Pectins, complex polysaccharides and major components of the plant primary cell wall, can be degraded by pectate lyases (PLs). PLs cleave glycosidic bonds of homogalacturonans (HG), the main pectic domain, by β-elimination, releasing unsaturated oligogalacturonides (OGs). To understand the catalytic mechanism and structure/function of these enzymes, we characterized VdPelB from *Verticillium dahliae*. We first solved the crystal structure of VdPelB at 1.2Å resolution showing that it is a right-handed parallel β-helix structure. Molecular dynamics (MD) simulations further highlighted the dynamics of the enzyme in complex with substrates that vary in their degree of methylesterification, identifying amino acids involved in substrate binding and cleavage of non-methylesterified pectins. We then biochemically characterized wild type and mutated forms of VdPelB. Pectate lyase VdPelB was most active on non-methylesterified pectins, at pH8.0 in presence of Ca^{2+} ions. The VdPelB-G125R mutant was most active at pH9.0 and showed higher relative activity compared to native enzyme. The OGs released by VdPelB differed to that of previously characterized PLs, showing its peculiar specificity in relation to its structure. OGs released from *Verticillium*-partially tolerant and sensitive flax cultivars differed which could facilitate the identification VdPelB-mediated elicitors of defence responses.

1   **The specificity of pectate lyase VdPelB from *Verticilium dahliae* is highlighted by**

2   **structural, dynamical and biochemical characterizations**

3

4   Josip Safran[1], Vanessa Ung[2], Julie Bouckaert[3], Olivier Habrylo[1], Roland Molinié[1], Jean-Xavier

5   Fontaine[1], Adrien Lemaire[1], Aline Voxeur[4], Serge Pilard[5], Corinne Pau-Roblot[1], Davide

6   Mercadante[2], Jérôme Pelloux[1*], Fabien Sénéchal[1*]

7

8

9   [1] : UMRT INRAE 1158 BioEcoAgro – BIOPI Biologie des Plantes et Innovation, Université

10   de Picardie, 33 Rue St Leu, 80039 Amiens, France. [2] : School of Chemical Sciences, The

11   University 9 of Auckland, Private Bag 92019, Auckland 1142, New Zealand. [3] : UMR 8576

12   Unité de Glycobiologie Structurale et Fonctionnelle (UGSF) IRI50, Avenue de Halley, 59658

13   Villeneuve d'Ascq, France. [4] : Université Paris-Saclay, INRAE, AgroParisTech, Institut Jean-

14   Pierre Bourgin (IJPB), 78000, Versailles, France. [5] : Plateforme Analytique, Université de

15   Picardie, 33, Rue St Leu, 80039 Amiens, France.

16   *contributed equally as last authors

17   **<u>Corresponding author:</u>** Fabien Sénéchal (fabien.senechal@u-picardie.fr) and Jérôme Pelloux

18   (jerome.pelloux@u-picardie.fr)

19   UMR INRAE 1158 BioEcoAgro-Biologie des Plantes et Innovation, Université de Picardie

20   Jules Verne, UFR des Sciences, 33 Rue St Leu, 80039 Amiens, France

21

Abstract

Pectins, complex polysaccharides and major components of the plant primary cell wall, can be degraded by pectate lyases (PLs). PLs cleave glycosidic bonds of homogalacturonans (HG), the main pectic domain, by β-elimination, releasing unsaturated oligogalacturonides (OGs). To understand the catalytic mechanism and structure/function of these enzymes, we characterized VdPelB from *Verticillium dahliae*. We first solved the crystal structure of VdPelB at 1.2Å resolution showing that it is a right-handed parallel β-helix structure. Molecular dynamics (MD) simulations further highlighted the dynamics of the enzyme in complex with substrates that vary in their degree of methylesterification, identifying amino acids involved in substrate binding and cleavage of non-methylesterified pectins. We then biochemically characterized wild type and mutated forms of VdPelB. Pectate lyase VdPelB was most active on non-methylesterified pectins, at pH8.0 in presence of Ca^{2+} ions. The VdPelB-G125R mutant was most active at pH9.0 and showed higher relative activity compared to native enzyme. The OGs released by VdPelB differed to that of previously characterized PLs, showing its peculiar specificity in relation to its structure. OGs released from *Verticillium*-partially tolerant and sensitive flax cultivars differed which could facilitate the identification VdPelB-mediated elicitors of defence responses.

Keywords: Pectate lyase, pectins, homogalacturonan, oligogalacturonides, *Verticillium dahliae*.

1. Introduction

Primary cell wall, a complex structure of proteins and polysaccharides, cellulose and hemicelluloses, is embedded in a pectin matrix. Pectins, are complex polysaccharides composing up to 30% of cell wall dry mass in dicotyledonous species [1]. Pectin is mainly constituted of homogalacturonan (HG), rhamnogalacturonan I (RG-I) and rhamnogalacturonan II (RG-II) domains, but its composition can differ between plant organs and among species. The most abundant pectic domain is HG, a linear homopolymer of α-1,4-linked galacturonic acids (GalA), which represents up to 65% of pectins [2]. During synthesis, HG can be O-acetylated at O-2 or O-3 and/or methylesterified at C-6 carboxyl, before being exported at the cell wall with a degree of methylesterification (DM) of ~80% and a degree of acetylation (DA) of ~5-10%, depending on species [3]. At the wall, HG chains can be modified by different enzyme families, including pectin acetylesterase (PAEs; EC 3.1.1.6), pectin methylesterases (PMEs; CE8, EC 3.1.1.11), polygalacturonases (PGs; GH28, EC 3.2.1.15, EC 3.2.1.67, EC 3.2.1.82), and pectin lyases-like (PLLs), which comprise pectate lyases (PLs; EC 4.2.2.2) and pectin lyase (PNLs, EC 4.2.2.10). All these enzymes are produced by plants to fine-tune pectin during development [4–8], but they are also secreted by most phytopathogenic bacteria and fungi during plant infection [9–13]. PMEs and PAE hydrolyse the O6-ester and O2-acetylated linkages, respectively, leading to a higher susceptibility of HG to PG- and PLL-mediated degradation [14]. PLL are pectolytic enzymes that cleave HG via a β-elimination mechanism leading to the formation of an unsaturated C4-C5 bond [15], and can be divided into two subfamilies depending on their biochemical specificities: i) PLs have a high affinity for non- or low-methylesterified pectins and an optimal pH near 8.5. Their activity requires Ca^{2+} ions. ii) PNLs are most active on high-DM pectins at acidic pH values [16]. Both type of enzymes can degrade HG chains, and release oligogalacturonides (OGs), but their mode of action can differ. For PLs both endo and exo modes of action have been described, while only endo-PNL have been characterised so far [17]. For the latter, it was notably shown that endo-PNLs from *B. fuckeliana*, *A. parasiticus* and *Aspergillus* sp., can first release OGs with degrees of polymerisation (DP) 5–7, that are subsequently used as substrates, generating OGs of DP3 and DP4 as end-products [9,18,19]. Despite having the same DP, the final products can differ in their degrees and patterns of methylesterification and acetylation (DM/DA) depending on the enzymes' specificities; implying potential differences in substrate binding, and therefore in PLLs fine structures. Several crystallographic structures of bacterial and fungal PLL have been reported [15,20–24]. Overall, the PLL fold resemble that of published PME, PGs and

78 rhamnogalacturonan lyases [25–27], and is composed of three parallel β-sheets forming a right-

79 handed parallel β-helix. The three β-sheets are called PB1, PB2 and PB3 and the turns

80 connecting them T1, T2 and T3 [28]. The active site features three Asp, localized on the PB1

81 β-sheet and, in the case of PLs, accommodates Ca^{2+} [29]. In PNLs, Ca^{2+} is, on the other hand,

82 replaced by Asp [15]. Additionally, the PL binding site is dominated by charged acidic and

83 basic residues (Gln, Lys, Arg) which can accommodate negatively charged pectate substrates.

84 In contrast, the PNL binding site is dominated by aromatic residues [15,29], which have less

85 affinity for lowly methylesterified pectins. These differences in structure could translate into

86 distinct enzyme dynamics when in complex with substrates of varying degrees of

87 methylesterification.

88   In fungi, PLLs are encoded by large multigenic families which are expressed during

89 infection. *Verticillium dahliae* Kleb., a soil-borne vascular fungus, targets a large number of

90 plant species, causing Verticillium wilt disease to become widespread among fiber flax, with

91 detrimental effects to fiber quality [30–32]. *V. dahliae* infects plants by piercing the root surface

92 using hyphae. When Verticillium reaches the vascular tissue, hyphae start to bud and form

93 conidia which progress in xylem vessels before germinating and penetrating adjacent vessel

94 elements to start another infection cycle. [33,34]. During its colonization and proliferation

95 Verticillium produces and secretes a number of pectinolytic enzymes, including thirteen PLLs.

96 Considering the role of PLLs in determining pathogenicity, it is of paramount importance to

97 determine their biochemical and structural properties [30,35,36]. This could allow engineering

98 novel strategies to control or inhibit, the pathogen's pectinolytic arsenal. For this purpose, we

99 characterized, via combined experimental and computational approaches, one *V. dahliae* PLL

100 (VdPelB, VDAG_04718) after its heterologous expression in *P. pastoris*. The obtention of the

101 3D structure of VdPelB after X-ray diffraction and the analysis of enzyme dynamics when in

102 complex with substrates of distinct DM, allowed the identification of the residues favouring

103 pectate lyase (PL) activity. Experiments confirmed the importance of these residues in

104 mediating PL activity showing that VdPelB is a *bona fide* PL, that releases peculiar OG as

105 compared to previously characterized PLs. More importantly, the OGs released from roots of

106 *Verticillium*-partially tolerant and sensitive flax cultivars differed, paving the way for the

107 identification of VdPelB-mediated OGs that can trigger plant defence mechanisms.

108

109 **2. Material and methods**

110   **2.1. Bioinformatical analysis**

4

Verticillium dahliae PLL sequences were retrieved using available genome database (ftp.broadinstitute.org/). SignalP-5.0 Server (http://www.cbs.dtu.dk/services/ SignalP/) was used for identifying putative signal peptide and putative glycosylation sites were predicted using NetOGlyc 4.0 Server (http://www.cbs.dtu.dk/services/NetOGlyc/). Sequences were aligned and phylogenetic analysis was carried out using MEGA multiple sequence alignment program (https://www.megasoftware.net/). Homology models used for molecular replacement were created using I-TASSER structure prediction software (https://zhanglab.ccmb.med.umich.edu/I-TASSER/) and UCSF Chimera (http://www.cgl.ucsf.edu/chimera/) was used for creation of graphics.

2.2. Fungal strain and growth

V.dahliae was isolated from CALIRA company flax test fields (Martainneville, France) and was kindly provided by Linéa-Semences company (Grandvilliers, France). Fungus was grown as described in Safran et al. [37]. Briefly, fungus was grown in polygalacturonic acid sodium salt (PGA, P3850, Sigma) at 10 g.L^{-1} and in pectin methylesterified potassium salt from citrus fruit (55–70% DM, P9436, Sigma) solutions to induce expression of PLLs. After 15 days of growth in dark conditions at 25°C and 80 rpm shaking, mycelium was collected and filtered under vacuum using Buchner flask. Collected mycelium was frozen in liquid nitrogen, lyophilized and ground. Isolation of RNA and cDNA synthesis was realized as previously described in Lemaire et al.[38].

2.3. Cloning, heterologous expression and purification of VdPelB

V. dahliae PelB gene (VdPelB, UNIPROT: G2X3Y1, GenBank: EGY23280.1, VDAG_04718) consists of 1 single exon of 1002 bp length. The coding sequence, minus the nucleotides encoding signal peptide, was PCR-amplified using cDNA and gene-specific primers while VdPelB mutants were generated by PCR mutagenesis, a method for generating site-directed mutagenesis, using specific primers carrying mutations (Table S1). Cloning of the PCR-amplified sequences in pPICZαB, sequencing and expression in P. pastoris heterologous expression system as well as purification steps were done as previously described in Safran et al. [37].

2.4. Crystallization of VdPelB

Pectate lyase VdPelB was concentrated at 10 mg.mL^{-1} in Tris-HCl pH–7.5 buffer. Crystallization conditions were screened using the sitting-drop vapor-diffusion method. Pectate

5

lyase VdPelB (100 nL) was mixed with an equal volume of precipitant (1:1) using Mosquito robot (STP Labtech). The crystals that resulted in best diffraction data were obtained with 0.1 M MIB (Malonic acid, Imidazole, Boric acid system) at pH8.0, with 25 % PEG 1500 as the precipitant (condition B5 from the PACT premier kit, Molecular Dimensions, Sheffield, UK) after 1 month. Optimization was realized using the hanging drop vapor-diffusion method forming the drop by mixing 1 µL of precipitant solution with 1 µL of the enzyme. The crystals (120 µm x 30 µm) were cryo-protected by increasing PEG 1500 concentration to 35%, before mounting them in a loop and flash-cooling them in liquid nitrogen.

2.5. VdPelB X-ray data collection and processing

X-ray diffraction data were collected at the PROXIMA-2a beamline of the Soleil synchrotron (Saint Aubin, France), at a temperature of -173°C using an EIGER 9M detector (Dectris). Upon a first data collection to 1.3 Å resolution, three more data sets were collected from the same crystal in order to obtain a complete data set. Thereby the kappa angle was tilted once to 30°, once to 60° and finally a helical data set was collected at 1.2 Å resolution. The reflections of each data set were indexed and integrated using XDS [39], scaled and merged using XSCALE [40]. The VdPelB crystal has a primitive monoclinic lattice in the P 1 2_1 1 space group, with two molecules contained in asymmetric unit [41].

2.6. Structure solution and refinement

The structure of VdPelB was solved by molecular replacement using *Phaser* [42]. The data were phased using pectate lyase BsPelA (PDB: 3VMV, Uniprot D0VP31), as a search model [43]. Model was build using *Autobuild* and refined using *Refine* from PHENIX suite [44]. The model was iteratively improved with *Coot* [45] and *Refine.* The final structure for VdPelB has been deposited in the Protein Data Bank (PDB) as entry 7BBV.

2.7. VdPelB biochemical characterization

Pierce BCA Protein Assay Kit (Thermo Fisher Scientific, Waltham, Massachusetts, United States) was used to determine the protein concentration, with Bovine Serum Albumin (A7906, Sigma) as a standard. Deglycosylation was performed using Peptide-N-Glycosidase F (PNGase F) at 37 °C for one hour according to the supplier's protocol (New England Biolabs, Hitchin, UK). Enzyme purity and molecular weight were estimated using a 12% SDS-PAGE and mini-PROTEAN 3 system (BioRad, Hercules, California, United States). Gels were stained using

172 PageBlue Protein Staining Solution (Thermo Fisher Scientific) according to the manufacturer's

173 protocol.

174   The substrate specificity of VdPelB was determined using PGA (81325, Sigma) and citrus

175 pectin of various DM: 20–34% (P9311, Sigma), 55–70% (P9436, Sigma) and >85% (P9561,

176 Sigma), with 0.5 μM $CaCl_2$ or 5 μM EDTA (Sigma) final concentrations. Enzyme activity was

177 measured by monitoring the increase in optical density at 235 nm due to formation of

178 unsaturated uronide product using UV/VIS Spectrophotometer (PowerWave Xs2, BioTek,

179 France) during 60 min. The optimum temperature was determined by incubating the enzymatic

180 reaction between 20 and 70°C for 12 min using PGA as a substrate (0.4%, w/v). The optimum

181 pH was determined between pH5.0 and 10.0 using sodium phosphate (NaP, pH5.0 to 7.0) and

182 Tris-HCl buffer (pH7.0 to 10.0) and 0.4% (w/v) PGA as a substrate. VdPelB and VdPelB-

183 G125R kinetic parameters, K_m, V_{max} and k_{cat}, were calculated using GraphPad Prism (8.4.2).

184 The reactions were performed using 0.75 to 15 mg.mL^{-1} PGA concentrations at 50 mM Tris-

185 HCl pH8.0 (native) and 9.0 (G125R) during 12 min at 35°C. All experiments were realized in

186 triplicate. The statistical analysis was done using the Welch's t-test.

2.8. Digestion of commercial pectins and released OGs profiling

188   OGs released after digestions by recombinant VdPelB or commercially available

189 Aspergillus PL (named AsPel) were identified as described in Voxeur et al., 2019 [9], using a

190 novel in-house OGs library. Briefly, DM 20–34% (P9311, Sigma) and sugar beet pectin with

191 DM 42% and degree of acetylation (DA) 31% (CP Kelco, Atlanta, United States) were prepared

192 at 0.4 % (w/v) final concentration diluted in 50 mM Tris-HCl buffer (pH8.0) and incubated

193 with either VdPelB or AsPel (E-PCLYAN, Megazyme). For each substrate, enzyme

194 concentrations were adjusted to have enzymes at iso-activities (Table S2). For each substrate

195 two dilutions, were used for analysing OGs released in early, VdPelB-2 and AsPel-2, and late

196 phase, VdPelB-1 and AsPel-1, of digestions. Digestions were performed overnight. Non-

197 digested pectins were pelleted by centrifugation and the supernatant dried in a speed vacuum

198 concentrator (Concentrator plus, Eppendorf, Hamburg, Germany). Separation of OGs was done

199 as previously described using an ACQUITY UPLC Protein BEH SEC column (125Å, 1.7 μm,

200 4.6 mm x 300 mm) at a flow rate of 0.4 ml min^{-1}. MS detection was performed using an

201 ACQUITY UPLC H-Class system coupled to a SYNAPT G2-Si-Q-TOF hybrid quadrupole

202 time-of-flight instrument (Waters) equipped with an electrospray ionization (ESI) source (Z-

203 spray) and an additional sprayer for the reference compound (lock spray). Samples were

204 analysed by ESI–high-resolution MS (HRMS) and MS/MS in negative ionization mode. Data

205 acquisition and processing were performed with MASSLYNX software (v.4.1; Waters).
206 [9,37,46].

207 The intensities were defined as the area under the curve, for each OG. Peak areas were clustered
208 by hierarchical clustering with complete linkage on the euclidian distance matrix and visualized
209 in the heatmap-package using R version 3.6.0. The statistical analysis was done using the
210 Welch's t-test.

2.9. Molecular Dynamics simulations

212 Two sets of molecular dynamics (MD) simulations were conducted on the VdPelB protein:
213 one in complex with a fully non-methylesterified polygalacturonate decasaccharide, and the
214 other with a fully methylesterified polygalacturonate decasaccharide. Parameters specified by
215 the AMBER14SB_parmbsc1 forcefield [47] were used to create the molecular topologies of
216 the complexes. Each complex was set up in a cubic box with solute-box distances of 1.0 nm
217 and solvated with water molecules specific to the TIP3P water model [48]. Na^+ and Cl^- ions
218 were added to neutralise the system's net charge and reach a salt concentration of 0.165 M.
219 Using a steep-descent algorithm with a step size of 0.01, energy minimisation was performed
220 to resolve clashes between particles, with convergence being established at a particle-particle
221 force of 1000 kJ mol-1 nm-1. Particle-particle forces were calculated by considering van der
222 Waals and electrostatic interactions occurring up to 1.0 nm, as well as long-range electrostatics
223 treated in the Fourier space using the Particle Mesh Ewald (PME) summation method. Solvent
224 equilibration was attained post minimisation in two stages: through the NVT and NPT
225 ensembles, to reach constant temperature and pressure, respectively. Equilibration of the
226 solvent under the NVT ensemble was conducted for 1 ns, integrating the equation of motion at
227 a time step of 2 fs. The target reference temperature was 310.15 K, coupled every 0.1 ps using
228 the V-rescale thermostat3. Based on the Maxwell-Boltzmann distribution [49] at 310.15 K,
229 random velocities were then assigned to each particle in the system. Finally, solvent
230 equilibration under the NPT ensemble was conducted for 1 ns, continuing from the last step of
231 the previous equilibration, in terms of particle coordinates and velocities, at a reference
232 temperature of 310.15 K, coupled every 0.1 ps using the V-rescale thermostat [50]. Here,
233 pressure coupling was isotropically coupled every 2.0 ps, at 1 bar, using the Parrinello-Rahman
234 barostat [51]. Particle-particle interactions were computed by constructing pair lists using the
235 Verlet scheme. Short-range van der Waals and electrostatic interactions sampled through a
236 Coulomb potential, were calculated at a cutoff of 1.0 nm. The PME algorithm [52] was used to
237 compute long-range electrostatic interactions beyond this cut-off in the Fourier space, utilising

a Fourier grid spacing of 0.16 and a cubic B-spline interpolation level at 4. The simulations were then performed on in-house machines, using GROMACS (Groningen Machine for Chemical Simulations) version 2021.37. Each set of simulations were run for 150 ns each, at a time step of 2 fs, with molecular dynamics trajectories written out every 10 ps. Simulations were replicated 7 times for a total production run time of 1.05 μs per complex. Replicates differed with respect to the random particle velocity sets computed under the NVT ensemble. For analysis, the first 50 ns of each production run were discarded as equilibration time. In-house Python 3 scripts implemented using Jupyter notebooks [53] were used to carry out analyses. Figures were created and rendered with Matplotlib [54] and VMD (Visual Molecular Dynamics)[55].

3. Results and Discussion

3.1. Sequence and phylogeny analysis

In addition to 9 polygalacturonases (PGs) and 4 pectin methylesterases (PMEs), *V. dahliae* encodes 30 putative endo-pectate lyases (EC 4.2.2.2), exo-pectate lyases (EC 4.2.2.9), endo-pectin lyases (EC 4.2.2.10), belonging to PL1-PL3 and PL9 families, respectively [56]. For hierarchical clustering of Verticilium's sequences with other PLLs, fifty-one amino acid sequences encoding putative PLLs, belonging to bacteria, fungi and plants were aligned and a phylogenetic tree was built. Different clades can be distinguished. (**Fig. 1**). *V. dahliae* PelB (VdPelB, VDAG_04718) clustered with VDAG_05344 (59.68% sequence identity) with close relations to VDAG_05402 (57.19% sequence identity) and VDAG_07566 (56.95% sequence identity). VDAG_05402 and VDAG_05344, that are found in the protein secretome, have orthologs in *V. alfalfa* (VDBG_07839 and VDBG_10041), which were shown to possess putative lyase activity [36,57]. Plant PLLs from *A. thaliana* (AtPLL21, AtPLL15 and AtPLL18) formed a separate clade with close connections to *A. denitrificans* (AdVexL), a PLL homologue [58]. *D.dadanti* (DdPelI), *Bacillus Sp.* KSM-P15 (BsPel-P15) and *C. bescii* (CbPel1854) formed separate clades similarly to *B.subtilis* and *D. dadantii PLs* (BsPel, DdPelA and DdPelC). The clade corresponding to PNLs consisting of *A. tubingensis* PelA (AtPelA), *A. niger* (AnPelA, AnPnlA and AnPelB), *A. luchuensis* AlPelB was closely related to VDAG_07238 and VDAG_08154 which were indeed annotated as putative PNLs [18,56]. VDAG_06155 was previously named VdPel1 and previously characterized as a pectate lyase [35].
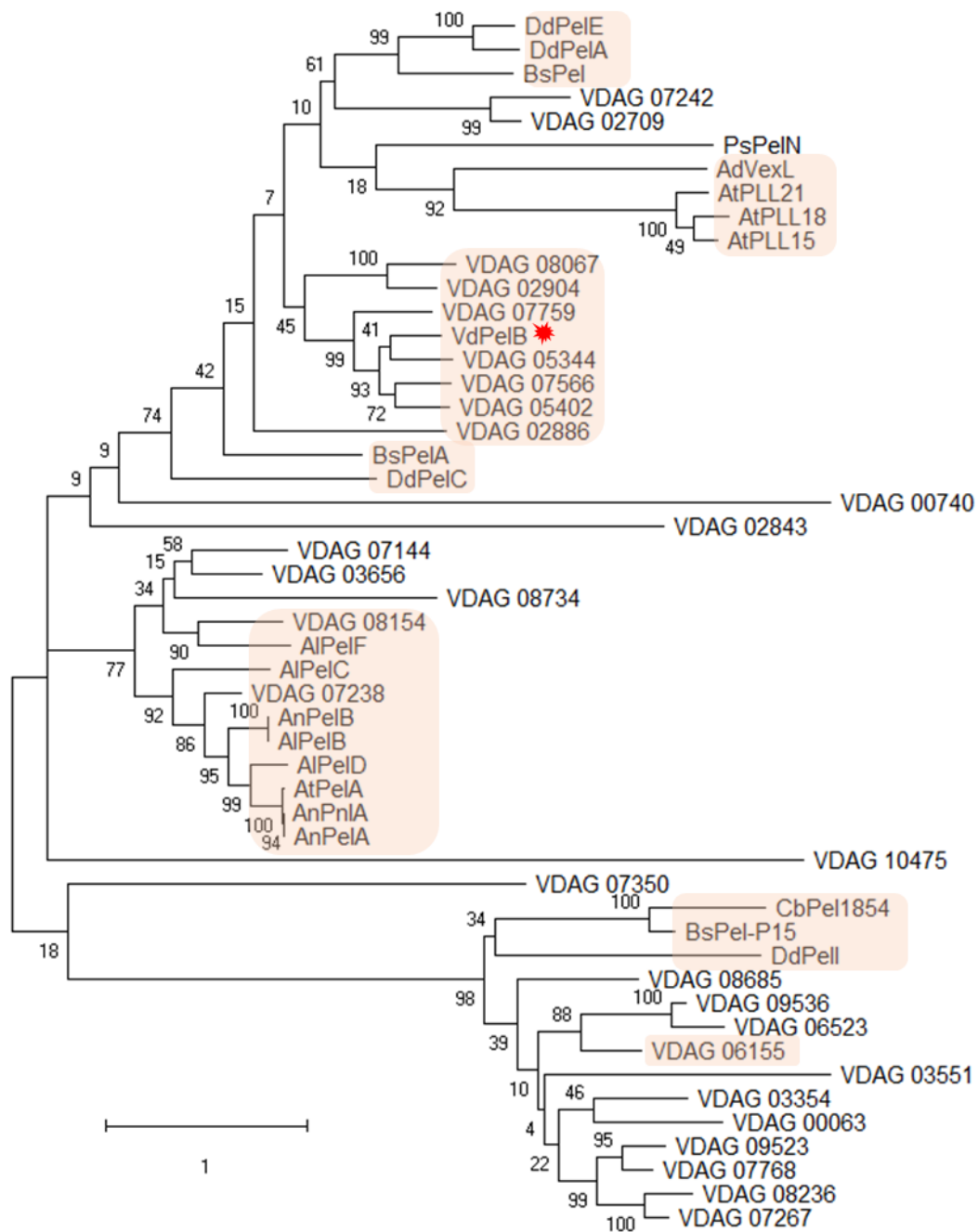
Fig. 1. Phylogenetic analysis of *V. dahliae pectate lyase* VdPelB with selected PLLs

Phylogentic tree representing *V. dahliae* VdPelB (VDAG_04718, G2X3Y1, red star) amino acid sequence in comparison with PLLs from Verticillium [VDAG_00740 (G2WQU8), VDAG_02904 (G2WXC5), VDAG_05344 (G2X628), VDAG_07242 (G2XBA4), VDAG_07759 (G2XC77), VDAG_02709 (G2WWT0), VDAG_02843 (G2WX64), VDAG_02886 (G2WXA7), VDAG_03656 (G2X1P5), VDAG_05402 (G2X597), VDAG_07144 (G2X9U9), VDAG_07238 (G2XBA0), VDAG_07566 (G2XBY8), VDAG_08067 (G2XD35), VDAG_08154 (G2XDC2), VDAG_08734 (G2XF02), VDAG_10475 (G2XJZ3), VDAG_03354 (G2WZB2), VDAG_03551 (G2WZV9), VDAG_07267 (G2XBC9), VDAG_07768 (G2XC86), VDAG_08236 (G2XDK4), VDAG_06155 (G2X8L4), VDAG_06523 (G2X7R5), VDAG_08685 (G2XEV0), VDAG_09523 (G2XH91), VDAG_09536 (G2XHA4), VDAG_00063 (G2WR80), VDAG_07350 (G2XGG7)], *Arabidopsis thaliana* [AtPLL15 (At5g63180), AtPLL18 (At3g27400), AtPLL21 (At5g48900)], *Dickeya dadanti* [DdPelA (P0C1A2), DdPelC

282 (P11073), DdPelE (P04960), DdPelI (O50325)], *Bacillus subtilis* [BsPel (P39116)], *Bacillus Sp*. KSM-P15
283 [BsPel-P15 (Q9RHW0)], *Bacillus sp*. N16-5 [BsPelA (D0VP31)], *Aspergillus niger* AnPelA [(Q01172), AnPelB
284 (Q00205), AnPnlA (A2R3I1)], *Achromobacter denitrificans* [AdVexL (A0A160EBC2)], *Aspergillus tubingensis*
285 [AtPelA (A0A100IK89)], *Aspergillus luchuensis* [AlPelB (G7Y0I4)], *Acidovorax citrulli* [AcPel343, (A1TSQ3)],
286 *Paenibacillus sp*. 0602 [PsPelN (W8CR80)], *Caldicellulosiruptor bescii* [CbPel1854 (B9MKT4)]. Maximum
287 likelihood tree was constructed with 1000 bootstrap replicates. Most important clades are indicated in orange
288 squares while VdPelB is marked by red star. Amino acids sequences were retrieved from Uniprot and TAIR.

3.2. Expression and purification of VdPelB

290 Since the expression was performed using the pPICZαB vector with the yeast alpha-factor

291 directing VdPelB secretion in the culture media, the protein could be easily recovered and

292 purified. The protein is composed of 343 amino acids, including the 6xHIS tag at the C-terminus

293 used for affinity chromatography purification. After purification, VdPelB purity was assessed

294 using SDS-PAGE with an apparent molecular mass of ~38 kDa (**Fig. S1**), higher than what was

295 predicted on the basis of the amino acid sequence (33.8 kDa). However, this shift is likely to

296 correspond to the two tags that are fused to the protein (His and C-myc) and to the presence of

297 19 putative O-glycosylation sites, as predicted by NetOGlyc 4.0 Server.

3.3. VdPelB has a right-handed parallel β-helix fold

299 Pectate lyase VdPelB was crystallized and its 3D structure was determined using X-ray

300 diffraction. VdPelB crystallized in monoclinic P 1 2$_1$ 1 asymmetric unit. Four data sets,

301 collected from the same crystal at 1.2 Å resolution, were integrated, scaled and merged. There

302 are two molecules in the asymmetric units: chains A and B are highly similar with a Cα root

303 mean square deviation (rmsd) value of 0.227 Å (**Fig. S2A**). The VdPelB structure consists of

304 298 amino acids with 18 at the N-terminus and 27 amino acids at the C-terminus that were not

305 resolved because of poor electron densities, while overall electron densities were well defined.

306 While no N-glycosylation sites could be revealed on the VdPelB structure, six O-glycosylation

307 sites carrying mannose are visible for each molecule: T22, T44, T45, T46, S48 and T54, in

308 accordance with the shift in size previously observed (**Fig. S2A**). During data acquisition no

309 heating of the crystal was observed, as shown by low B factors and good occupancies (**Fig. S3A**

310 **and B**). The final models' geometry, processing and refinement statistics are summarized

311 (**Table 1**). The VdPelB's structure has been deposited in the Protein Data Bank as entry 7BBV.

312 **Table 1. Data collection, processing and refinement for VdPelB**

Characteristics	VdPelB
Data collection	
Diffraction source	PROXIMA2
Wavelength (Å)	0.980
Temperature (°C)	-100.15
Detector	DECTRIS EIGER X 9M
Crystal-to-detector distance (mm)	115.02
Rotation range per image (°)	0.1
Total rotation range (°)	360
Crystal data	
Space group	P1 21 1
a, b, c (Å)	60.89, 59.69, 93.87
$\alpha, \beta, \gamma,$ (°)	90.00, 96.35, 90.00
Subunits per asymmetric unit	2
Data statistics	
Resolution range (Å)	60.52-1.2 (1.243 - 1.2)
Total No. of reflection	8536161 (112943)
No. of unique reflection	207497 (19983)
No. of reflections, test set	10362 (1003)
R_{merge} (%)	0.1036 (4.709)
Completeness (%)	99.30 (96.11)
$(I/\sigma(I))$	18.03 (0.22)
Multiplicity	41.1 (5.6)
$CC_{1/2}$ (%)	1 (0.116)
Refinement	
R_{crys}/R_{free} (%)	17.3 / 19.7
Average B – factor (Å^2)	33.18
No. of non-H atoms	
Protein	9097
Ion	2
Ligand	234
Water	1052
Total	10385
R.m.s. deviations	
Bonds (Å)	0.013
Angles (°)	1.39
Ramachandran plot	
Most favoured (%)	95.1
Allowed (%)	4.90
Outlier (%)	-

313

The VdPelB has a right-handed parallel β-helix fold which is common in pectinases [59]. The β-helix is formed by three parallel β-sheets - PB1, PB2 and PB3 which contain 7, 10 and 8 β-strands, respectively. Turns connecting the PB1-PB2, PB2-PB3 and PB3-PB1 β-sheets are named T1-turns, T2-turns and T3-turns, respectively, according to Yoder and Jurnak (**Fig. 2A, S4A and B**) [60]. T1-turns consist of 2-14 amino acids and builds the loop around the active site on the C-terminus. T2 turns mostly consist of 2 amino acids with Asn being one of the predominant amino acid, forming an N-ladder with the exception of an N245T mutation in VdPelB [15,20]. Pectate lyase VdPelB has a α-helix on N-terminus end that shields the hydrophobic core and is commonly conserved in PLs and PGs [15,61], while the C–terminus end is also protected by tail-like structure carrying one α-helix. Interestingly N- and C- terminus tails pack against PB2 (**Fig. 2A**). There are only two Cys (C25 and C137) that do not form a disulphide bridge.

Sequence and structural alignments show that VdPelB belong to the PL1 family. The VdPelB shares the highest structural similarity with BsPelA (PDB: 3VMV), with 30.06% sequence identity and Cα rmsd of 1.202 Å. The second-best structural alignment was with DdPelC (PDB: 1AIR) with 24.20% identity and Cα rmsd of 1.453 Å [43,62]. Both of these structures lack the long T3 loop described in *A.niger* pectate lyase (AnPelA, PDB: 1IDJ, **Fig. S2B** and **S5**) [15]. The putative active site is positioned between the T3 and T2 loops (**Fig. 2A and B**).
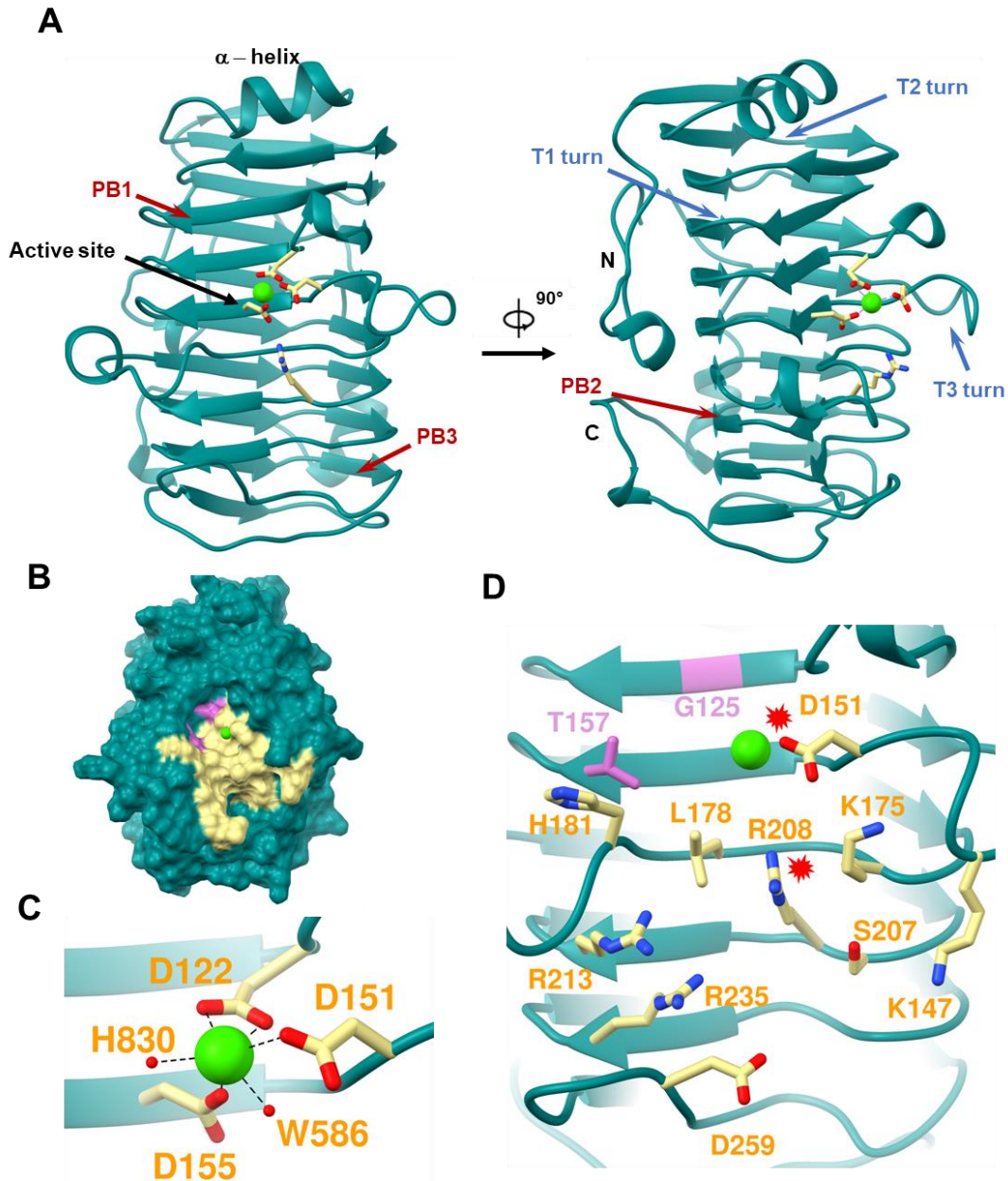
Fig. 2. Structure determination of VdPelB

A) Ribbon diagram of VdPelB crystalized in P1 21 1 space group. VdPelB is a right-handed parallel β helical structure consisting of β strands (red arrows) and turns (blue arrows). VdPelB active site's amino acids are yellow-colored while Ca atom is green. B) Surface representation of VdPelB binding groove. C) Active site of VdPelB highlighting conserved amino acids and atoms interacting with Ca. D) Structure of VdPelB binding groove highlighting amino acids involved in the interaction (yellow) and amino acids not of previously characterized in PLs (plum). Red stars indicate amino acids from the active site.

3.4. Active site harbours Ca^{2+} that is involved in catalysis

The VdPelB active site is well conserved, harbouring strictly conserved acidic and basic amino acids that are required for Ca^{2+} binding. Previously reported structures showed that two Asp (D122 and D155) and one Arg (R208) in VdPelB, are conserved, while D151 can be

14

mutated to Glu, or Arg in PNLs (**Fig. 2C** and **D**, Mayans et al., 1997). Other conserved amino acids in VdPelB include K175 and R213, with K175 being responsible for binding the carboxyl oxygen while R213 hydrogen bonds to C-2 and C-3 of GalA (**Fig. 2D**) [29,63]. Mutating any of these amino acids leads to decreased enzyme activity [64]. In VdPelB, Ca^{2+} ion is directly coordinated by D122, two carboxyl oxygen, D151, D155 and two water molecules (W568 and W830, **Fig. 2C**). In addition, mutation of D122T (VdPelB numbering) in BsPelA, is responsible for reduced affinity for Ca^{2+} [43]. In the catalytic mechanism, Ca^{2+} is directly involved in acidification of the proton absorption from C5 and elimination of group from C4, generating an unsaturated product. R208 act as a base, similarly to the hydrolysis in the reaction mechanism of the GH28 family [65,66].

3.5. Structural analysis of VdPelB suggests a PL activity mediated by peculiar specificities

The VdPelB binding groove comprises a number of basic and acidic amino acids including K147, D151, K175 L178, H181, S207, R208, R213 and R235 and D259 (**Fig. 2C and D**), that have previously been shown to be characteristics of PLs. This would suggest an enzyme activity on low DM pectins as amino acids positioned at the binding groove were indeed shown to differ between PNL and PL [15,21,24,29]. These amino acids are indeed mutated in Arg, Trp, Tyr, Gln and Gly in PNLs, which, by reducing their charge, would favour higher affinity for highly methylesterified pectins [15,29]. In VdPelB, as the T3 loop is missing, there are no equivalent to PNL specific W66, W81, W85, W151 amino acids (**Fig. S2B,** AnPelA numbering) and, moreover, W212 and W215 are replaced by K175 and L178 in VdPelB. In BsPelA and DdPelC, these amino acids are replaced by K177/K190 and L180/L193, highlighting the high conservation of amino acids in VdPelB/BsPelA/DdPelC and subsequently in PLs. When a DP4 ligand from DdPelC crystal structure is superimposed to VdPelB, hydrogen bonds and van der Waals interactions are visible with the above-mentioned amino acids (**Fig. S6)** [15,21,29,43].

Interestingly, despite this rather conserved PL-related binding groove, VdPelB harbors, in the vicinity of the active site, G125 and T157 that are not present in the well characterized DdPelC [62]. At these positions, DdPelC, which was shown to be a *bona fide* PL with a high activity on polygalacturonic acid and alkaline pH with Ca^{2+}-dependency, harbours Arg and Lys [15,63,67]. In that respect, the presence of G125 and T157 in VdPelB is similar to that identified in *Bacillus sp.* Pel-22, Pel-66, and Pel-90 and *Bacillus sp.* which showed activity on both PGA and high methylesterified pectins (**Fig. 2B** and **D**) [22,68,69]. The DdPelC amino acids being

overall positively charged, could explain the binding preference towards non-methylesterified, negatively charged substrates in the vicinity of the active site. In contrast, considering the size of Gly and Thr, they would sterically accommodate the increased size of methylesterified substrate. G125 and T157 could therefore account for a potential dual activity of VdPelB. Moreover, in previously characterized PLs and PNLs there is the presence of a small amino acids, Ser or Ala that replace H181. While H181 interacts directly with the substrate these amino acids do no provide this interaction instead the primary Ca^{2+} in the active site induce a substrate conformation that could be recognized by PLs [43]. Finally, L178 is positioned in-between the catalytic Ca^{2+} and R208 and is involved in substrate binding making it a perfect candidate to assess its importance (**Fig. 2D**).

3.6. Molecular dynamic simulations show higher dynamics of VdPelB in complex with methylesterified substrates

To determine how the structure of VdPelB and the observed differences in amino-acidic composition might influence the affinity with differently methylated substrates, we performed MD simulations on VdPelB in complex with either a non-methylesterified or fully methylesterified decasaccharides, which are able to occupy the entire binding groove (**Fig. 3**). MD simulations show substantially differential dynamic profiles for oligosaccharides with and without methylesterification. Expectedly, the dynamics is lowest in proximity of the catalytic subsite (+1) and increases consistently towards both the reducing and non-reducing ends of the substrate: with the highest dynamics found at the non-reducing end (**Fig. 3A**).

A quantitative estimation of the substrate dynamics was obtained by monitoring the root square mean fluctuations (RMSF) of each sugar residue and shows that a polygalacturonate substrate associates more stably in the subsites of the binding groove placed towards the sugar's reducing end (subsites -1 to -5), with differences between methylesterified and non-methylesterified substrates approaching the obtained standard deviation. In some cases, the dynamics reversed for non-methylesterified sugars, with a higher RMSF for de-methylesterified sugars towards the saccharide's reducing end (**Fig. 3B**). Moreover, and in line with an observed positively charged binding groove, non-methylesterified substrates retain a higher number of contacts than methylesterified sugars, with salt-bridges contributing the most to the observed differences (**Fig. 3C**).

We then additionally and specifically focused on the analysis of the interactions made by T157, which is nested with the -2 subsite of the binding groove. Simulations sample consistently

higher contacts formation between a methylesterified sugar docked in subsite -2 and T157, with distances shifted to lower values when compared to a non-methylesterified sugar (**Fig. 3D**), even the RMSF of non-methylesterified monosaccharides docked in subsite -2 experience on average, significantly lower dynamics. Altogether, the formation of a larger number of contacts between methylesterified saccharides docked in the -2 subsite suggests and active role of T157 in the binding of methylesterified chains: with the butanoic moiety of T157 engaging in hydrophobic interactions with the methyl-ester presented by methylesterified sugar units (**Fig. 3E**). While T157 is seen to have an active role in engaging with the substrate's hydrophobic moieties, an active role of G125, also in the same subsite, was not observed but it is plausible that the minimal size of G125 would increase the accommodability of methylesterified sugars in that position.
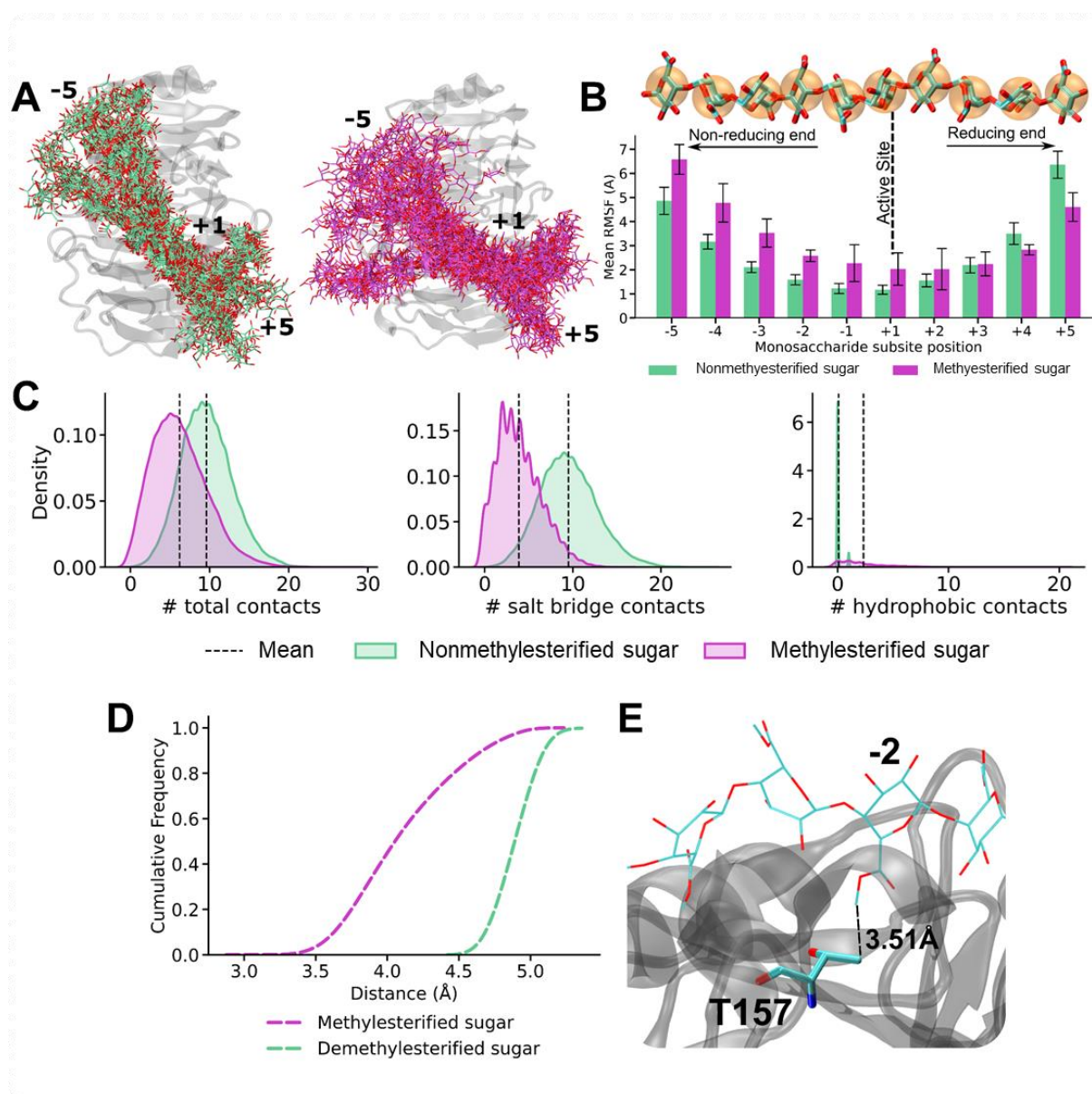
Fig. 3. VdPelB substrate dynamics in complex with fully de-methylesterified and methylesterified complex

A) Ensembles of non-methylesterified (green, left panel) and methylesterified (pink, right panel) HG decasaccharide at every 100 frames for the simulated VdPelB complexes. Substrate within the enzymes' binding grooves are labelled from -5 (HG-non-reducing end) to +5 (HG-reducing end) B) RMSF of non-methylesterified (green) and methylesterified (pink) HG bound across the binding groove of VdPelB. Numbers indicate the beta sheet position form the active site. C) Analysis of the contacts between VdPelB and non-methylesterified (green) and methylesterified substrate (pink). D) Distance between T157K residue and the substrate residues plotted as cumulative frequency. E) T157 hydrophobic interaction with methyl-ester of methylesterified substrate.

3.7. Biochemical characterization of VdPelB

We first determined the activity of VdPelB by following the release of 4,5-unsaturated bonds which can be detected at 235 nm using UV spectrophotometer. The VdPelB activity was first tested for its dependency towards Ca^{2+}. Using a standard PL assay, with PGA as a substrate, an increase in the VdPelB activity was measured in presence of calcium. In contrast in presence of EDTA, used as a chelating agent, no activity was detected, confirming the calcium-dependent activity of the enzyme **(Fig. S7A)** [15]. Activity measured in absence of added $CaCl_2$ reflects the presence of calcium from the culture media that is bound to VdPelB during production, and previously identified in the 3D structure. We tested the effects of increasing $CaCl_2$ concentrations and showed that the maximum activity was already reached when using as low as 0.125 μM **(Fig. S7B)**. To test the substrate-dependence of VdPelB, four substrates of increasing degrees of methyl-esterification were used. The VdPelB showed the highest activity on PGA, with less than 10% of the maximum activity measured on the three others substrates **(Fig. 4A)**. This shows that, as inferred from above-mentioned structural and dynamical data, The VdPelB act mainly as a PL although it can still show residual activity on high DM pectins. Considering this, PGA was used as substrate to test the pH-dependence of the enzyme's activity in sodium acetate and Tris-HCl buffers **(Fig. 4A)**. Pectate lyase VdPelB was most active at pH 8, with only a slight decrease in activity at pH 9 (93%). In contrast, the relative activity at pH 5-7 was close to null. The pH optimum for VdPelB was the same as *B. fuckeliana* Pel (pH 8) [70], close to that reported for *D. dadantii* PelN (pH 7.4) [71], but was lower to that measured for *B.clausii* Pel (pH 10.5) [72]. In contrast, the pH optimum was higher compared to five PNLs from *Aspergillus* sp. AaPelA (pH 6.1), AtPelA (pH 4.5), AtPelA (pH 6.4), AtPelD (pH 4.3) [18] and *A. parasiticus* Pel (pH 4) [19]. The optimum temperature assay showed that VdPelB was most active at 35°C **(Fig. S8)**. The VdPelB appeared less heat-tolerant as compared to thermophilic PLLs reported from Bacillus sp. RN1 90°C [73], *B. clausii* Pel, 70°C [72], *B. subtilis* Pel168, 50°C [74]. However, its optimum temperature is in the range of that measured

for *X. campestris* Pel [75] and cold-active Pel1 from *M. eurypsychrophila* [76]. The lack of disulphide bridges previously shown in the structure could be responsible for the lower stability of the enzyme at high temperatures, in comparison with previously characterized PLs [77].

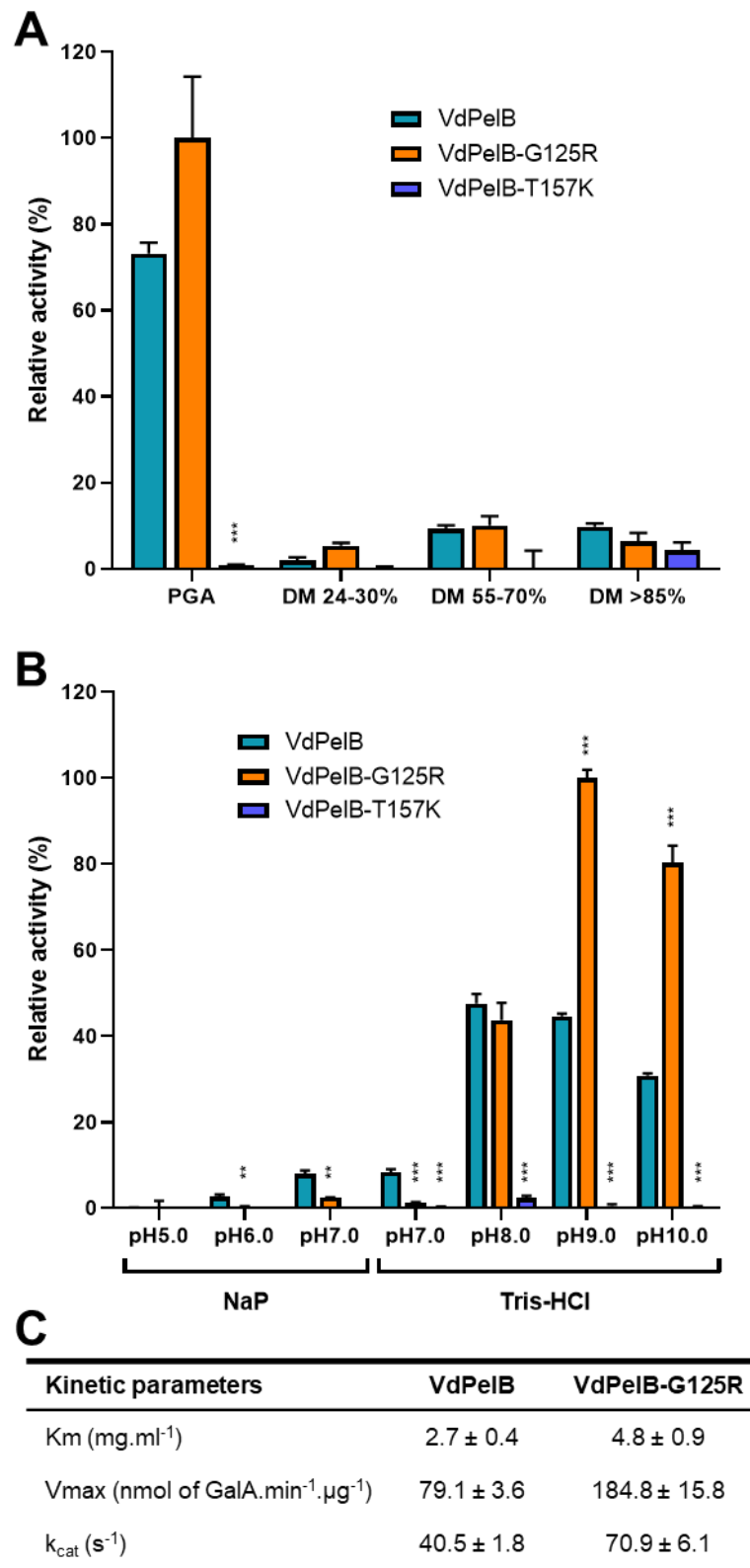| Kinetic parameters	VdPelB	VdPelB-G125R
K_m (mg.ml^{-1})	2.7 ± 0.4	4.8 ± 0.9
V_{max} (nmol of GalA.min^{-1}.µg^{-1})	79.1 ± 3.6	184.8 ± 15.8
k_{cat} (s^{-1})	40.5 ± 1.8	70.9 ± 6.1

Fig. 4. Biochemical characterization of VdPelB

461 A) Substrate-dependence of VdPelB, G125R and T157K. The activities were measured after 12 min of incubation
462 with PGA, pectins DM 24-30%, DM 55-70%, DM>85% with addition of Ca^{2+} at 35°C. B) pH-dependence of
463 VdPelB, G125R and T157K activity. The activities were measured after 12 min of incubation with PGA in sodium
464 phosphate (NaP) and Tris-HCl buffer at 35°C. Values correspond to means ± SD of three replicates. Welch t-test
465 comparing native with mutant VdPelB forms was used for statistical analysis. P value ***<0.001 and **<0.01. C)
466 Determination of Km, Vmax and kcat for ADPG2 and PGLR. Activity was assessed using various concentrations
467 of PGA at 35°C and pH8.0 (VdPelB) and pH9.0 (VdPelB-G125R).

3.8. Mutation of specific amino-acids affects VdPelB activity

469   Considering the structure of VdPelB and our hypothesis related to the role of some
470 amino acids in determining the mode of action of VdPelB, we generated mutated forms of the
471 enzyme for five amino acids that likely to be involved in the catalytic mechanism and/or
472 substrate binding: G125R, D151R, T157K, L178K and H181A. Enzymes were produced in *P.*
473 *pastoris* and purified (**Fig. S1**). If the importance of some of these amino acids (i.e. D151 and
474 H181) in the catalytic mechanism was previously shown for others PL [43,78], our study
475 highlights the key role of some novel amino acids in the catalytic mechanism. The activities of
476 mutants were tested at iso-quantities of wild-type enzyme. Surprisingly, the G125R mutant was
477 25% more active on PGA compared to the native enzyme and a shift in the optimum pH was
478 observed (**Fig. 4A**). While native enzyme was most active at pH8.0 with slight decrease in
479 activity at pH9.0, the activity of G125R mutant was approximately doubled at pH9.0 and
480 pH10.0 (**Fig. 4B**). Both enzymes kept the same activity at pH8.0. Moreover, using PGA as a
481 substrate, at 35°C, VdPelB and VdPelB-G125R differ slightly in their Km (2.7 versus 4.8
482 mg.ml^{-1}), Vmax (79.1 versus 184.8 nmol of GalA.min^{-1}.µg^{-1}) and kcat (40.5 versus 70.9 s^{-1},
483 **Fig. 4C**). The substitution of Gly with Arg, present in a number of previously characterized
484 PL could facilitate the interaction with the substrate and alkalinization of the active site thanks
485 to its physio-chemical properties [62]. Despite not knowing the exact rotamer orientation, the
486 presence of Arg with high pK$_a$ allowing strong hydrogen bonding and complex electrostatic
487 interactions within the active site, could change the optimal pH by acting on the protonation
488 state of amino acids involved in catalysis, as previously reported for a number of different
489 enzymes [65,79–82]. The activity of T157K was closed to null when tested on PGA and
490 different pHs. The introduction of a Lys, a chemically different and larger amino acids is likely
491 to introduce steric clashes notably with H181 and L178 that are important for the activity. The
492 H181A mutant lost much of its activity as there are less interaction/recognition with the
493 substrate. No activity for D151R and L178K mutants were observed in line with the fact that
494 D151 is an active site amino acid that binds the Ca^{2+}. Mutation of this amino-acid is negatively

impairing the functioning of the enzyme (**Fig. S7A** and **B**) [43,78]. We can hypothesize that L178K mutation positioned in between Ca^{2+}, R208 and the substrate, induces specific substrate conformation that diminishes the direct interaction between the enzyme catalytic centre and the substrate, which translates to loss of activity (**Fig. S9**).

3.9. Identification of the OGs released by VdPelB from commercial and cell wall pectins

To further understand the specificity of VdPelB on different substrates, we performed LC-ESI-MS/MS to determine the profiles of digestion products (OGs) and to compare with that of commercially available *Aspergillus sp.* Pel (AsPel, **Fig. S10**). To be fully comparable, digestions were realized, for each substrate, at iso-activities for the two enzymes. On the basis of digestion profiles, we identified 48 OGs and created a dedicated library that was used for identification and integration of peaks (**Table S3**). MS^2 fragmentation allowed determining the structure of some of the OGs (**Fig. S11** and **S12**). The OGs released by either of the enzymes mainly corresponded to 4,5-unsaturated OGs, which is in accordance with β-eliminating action of PLLs. When using pectins DM 20-34% and at low enzyme's concentration (VdPelB-2), VdPelB mainly released non-methylesterified OGs of high DP ($GalA_5$, $GalA_6$, $GalA_7$, $GalA_8$, $GalA_9$, $GalA_{10}$) that were subsequently hydrolysed when using more concentrated VdPelB (VdPelB-1, **Fig. 5A**). These digestion products strikingly differed to that generated by AsPel, that are methylesterified OGs of higher DP ($GalA_4Me_1$, $GalA_4Me_2$, $GalA_5Me_1$, $GalA_6Me_2$, $GalA_{11}Me_3...$), thus showing distinct enzymatic specificities. Altogether, these first results unequivocally shows both VdPelB and AsPel act as endo-PLs, but they differ in their processivity [9]. When using sugar beet pectins, that are known to be highly acetylated (DM 42%, DA 31%), VdPelB released acetylated OGs ($GalA_2Ac_2$, $GalA_3Ac_1$, $GalA_4Ac_1$, $GalA_5Ac_1$), while AsPel showed much lower activity and relative abundance of these OGs (**Fig. 5B**). Previous reports have shown that differences exist between PNL, in particular with regards to acetyl substitutions [18]. In contrast, AsPel released mainly methylesterifed OGs ($GalA_6Me_1$, $GalA_8Me_1$, $GalA_{10}Me_3...$).
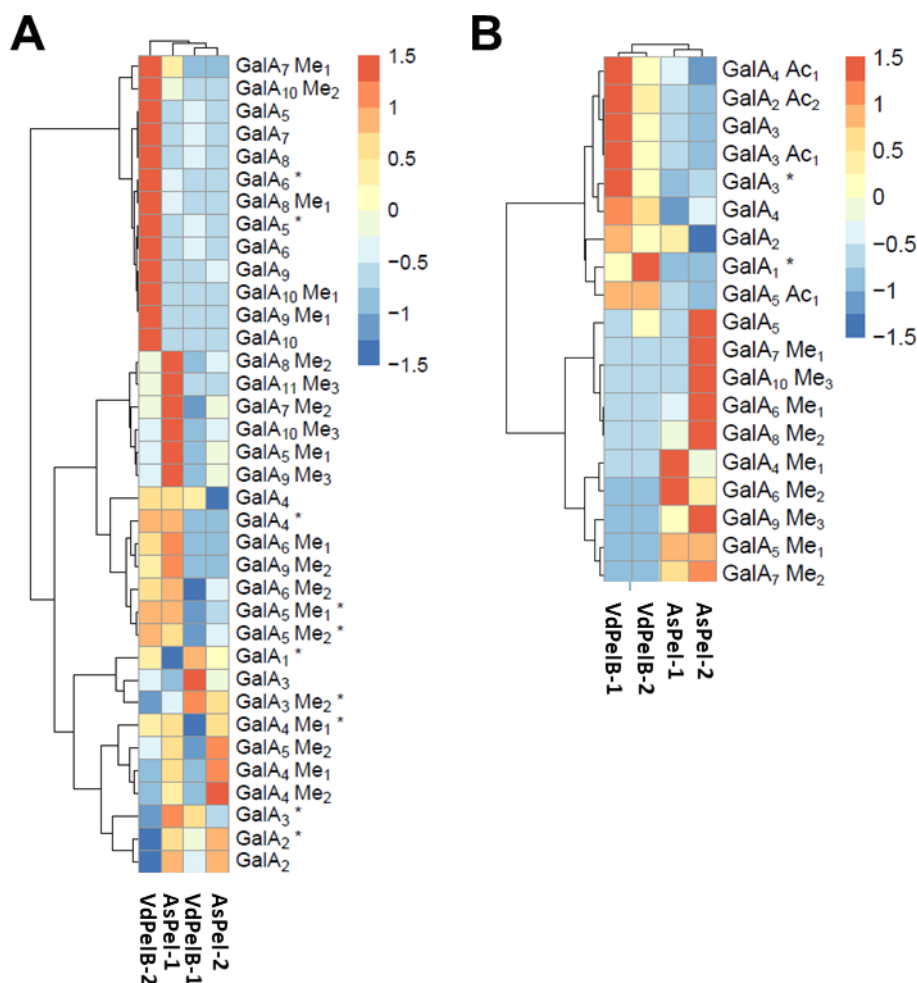
Fig. 5. Analysis of OGs produced by the action of VdPelB and AsPeI on pectins of various degrees of methylesterification and acetylation

OGs were separated by SEC and analysed by MS/MS. A) Pectins DM 24-30%. B) Sugar beet pectins (DM 42% DA 31%). Substrates were digested overnight at 40°C and pH8.0 using isoactivities of VdPelB and AsPel. Enzyme concentrations are stated in Table S2. Subscript numbers indicate the DP, DM and DA. * indicate non-unsaturated OGs. Values correspond to means of three replicates.

V. dahliae and closely related fungus from the same genus are known flax pathogens, where they use their enzymatic arsenal, that includes pectin degrading enzymes, for penetrating the host cell leading to infection [30]. To assess the potential role of VdPelB in flax pathogenicity we digested root cell walls from two flax cultivars, Evea (Verticillium-partially resistant), and Violin (Verticillium-susceptible), and we compared the OGs released. On root cell walls, VdPelB released mainly unsaturated OGs up to DP5 (**Fig. 6**). From similar starting root material, the OG total peak area detected was five times lower for Evea compared to Violin, suggesting that it is less susceptible to digestion by VdPelB. OGs released by VdPelB were mainly non-methylesterified but could be acetylated ($GalA_2$, $GalA_3$, $GalA_3Ac_1$, $GalA_4$,

GalA$_4$Ac$_1$ GalA$_5$, GalA$_5$Ac$_1$), and the abundance of GalA$_3$ and GalA$_4$ was five and fifteen times higher in Violin, respectively. These data together with that obtained from sugar beet pectins strongly suggests that VdPelB preference is for non-methylesterified and acetylated substrates. Our data suggest that cell wall structure differ between the two cultivars and that VdPelB could determine Verticillium pathogenicity thanks to a better degradation of the cell wall pectins of sensitive cultivars [37]. Similarly, VdPel1 was previously identified as virulence factor, where the deletion of this gene decreased virulence in tobacco, as compared with the wild-type Verticillium [35].
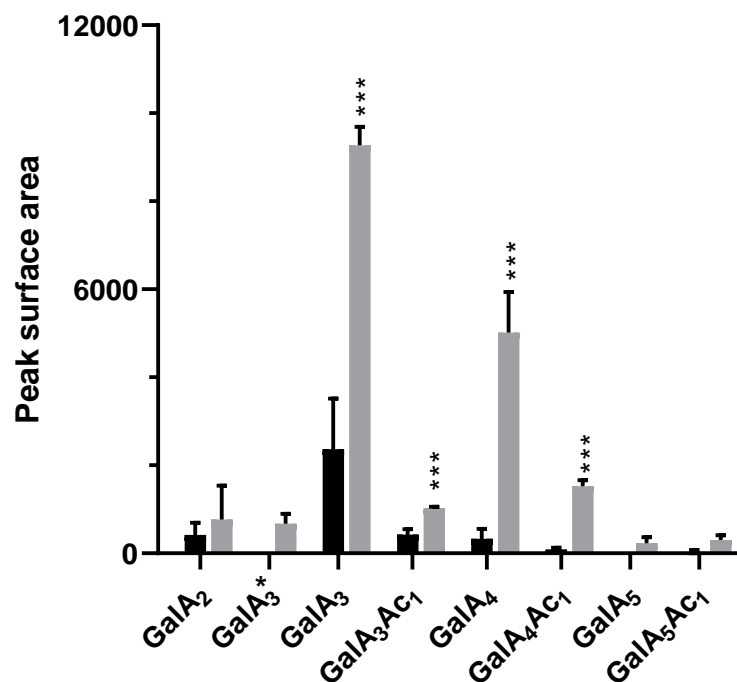

Fig. 6. Analysis of OGs released by VdPelB from flax roots.

The VdPelB was incubated overnight with roots from Évéa (spring flax, partially resistant to Verticillium wilt, black) and Violin (winter flax, more susceptible to Verticillium wilt, grey). Values correspond to means ± SD of three replicates. Welch t-test comparing Evea with Violin was used for statistical analysis. P value ***<0.001. Subscript numbers indicate the DP, DM and DA.

4. Conclusion

We have characterized, by multidisciplinary approaches, a novel pectinolytic enzyme from *V.dahliae*, VdPelB, that belongs to the PLL family. The protein was crystallised and its 3D structure determined at a high resolution. Pectate lyase VdPelB showed a conserved

559 structure, with parallel β-sheet topology for PLs and the active site harboured three conserved

560 Asp coordinating Ca^{2+} and Arg involved in the β-elimination mechanism. The binding groove

561 of VdPelB reveals conserved amino acids that are characteristic of PLs, with MD simulations

562 confirming the lower dynamics/higher affinity of the enzyme towards non-methylesterifed

563 pectins. As inferred from structural and dynamical analyses, VdPelB showed high activity on

564 non-methylesterified substrates, with a maximum activity at pH8.0 and 35°C. The analysis of

565 the structure led the identification, in the VdPelB, of peculiar amino acids that are normally

566 present in PNL. In particular, G125R mutant increased activity on PGA and switch in pH

567 optimum from 8.0 to 9.0 related to amino acids protonation. The analysis of the digestion

568 products showed that VdPelB act as an endo enzyme and that it can release a large diversity of

569 OGs with a preference for non-methylesterified and acetylated products. The OGs generated by

570 VdPelB from pectins extracted from Verticillium-partially tolerant and Verticillium-sensitive

571 flax cultivars showed that the enzyme could be a determinant of pathogenicity, since these OGs

572 differ as a function of pectins' structure. Thus, our study now paves the way for generating,

573 using dedicated enzymes, OG pools that could be used for protecting plants against

574 phytopathogens.

575

Author's contribution

Josip Safran: Conceptualization, Data curation, Formal analysis, Investigation, Methodology, Writing - original draft. **Vanessa Ung**: Data curation, Investigation, Methodology. **Julie Bouckaert**: Data curation, Investigation, Methodology. **Olivier Habrylo**: Formal analysis, Investigation, Methodology. **Roland Molinié**: Data curation, Formal analysis, Investigation, Methodology. **Jean-Xavier Fontaine**: Data curation, Formal analysis, Investigation, Methodology. **Adrien Lemaire**: Investigation, Methodology. **Aline Voxeur**: Investigation, Methodology. **Serge Pilard**: Investigation, Methodology. **Corinne Pau-Roblot** Conceptualization, Methodology. **Davide Mercadante**: Data curation, Methodology, Writing - review & editing. **Jérôme Pelloux**: Funding acquisition, Conceptualization, Writing - review & editing. **Fabien Sénéchal**: Conceptualization, Writing - review & editing.

Conflicts of interest

There are no conflicts of interest.

References

[1]   B.L. Ridley, M.A. O'Neill, D. Mohnen, Pectins: structure, biosynthesis, and oligogalacturonide-related signaling, Phytochemistry. 57 (2001) 929–967. https://doi.org/10.1016/S0031-9422(01)00113-3.

[2]   D. Mohnen, Pectin structure and biosynthesis, Curr. Opin. Plant Biol. 11 (2008) 266–277. https://doi.org/10.1016/j.pbi.2008.03.006.

[3]   M.A. Atmodjo, Z. Hao, D. Mohnen, Evolving views of pectin biosynthesis, Annu. Rev. Plant Biol. 64 (2013) 747–779. https://doi.org/10.1146/annurev-arplant-042811-105534.

[4]   Y. Rui, C. Xiao, H. Yi, B. Kandemir, J.Z. Wang, V.M. Puri, C.T. Anderson, POLYGALACTURONASE INVOLVED IN EXPANSION3 functions in seedling development, rosette growth, and stomatal dynamics in Arabidopsis thaliana, Plant Cell. 29 (2017) 2413–2432. https://doi.org/10.1105/tpc.17.00568.

[5]   C. Xiao, C. Somerville, C.T. Anderson, POLYGALACTURONASE INVOLVED IN EXPANSION1 functions in cell elongation and flower development in Arabidopsis, Plant Cell. 26 (2014) 1018–1035. https://doi.org/10.1105/tpc.114.123968.

[6]   J. Pelloux, C. Rustérucci, E.J. Mellerowicz, New insights into pectin methylesterase structure and function, Trends Plant Sci. 12 (2007) 267–277. https://doi.org/10.1016/j.tplants.2007.04.001.

[7]   F. Sénéchal, A. Mareck, P. Marcelo, P. Lerouge, J. Pelloux, Arabidopsis PME17 Activity can be Controlled by Pectin Methylesterase Inhibitor4, Plant Signal. Behav. 10 (2015) e983351. https://doi.org/10.4161/15592324.2014.983351.

[8]   V.S. Nocker, L. Sun, Analysis of promoter activity of members of the Pectate lyase-like(PLL) gene family in cell separation in Arabidopsis, BMC Plant Biol. 10 (2010) 152. https://doi.org/10.1186/1471-2229-10-152.

[9]   A. Voxeur, O. Habrylo, S. Guénin, F. Miart, M.C. Soulié, C. Rihouey, C. Pau-Roblot, J.M. Domon, L. Gutierrez, J. Pelloux, G. Mouille, M. Fagard, H. Höfte, S. Vernhettes, Oligogalacturonide production upon Arabidopsis thaliana-Botrytis cinerea interaction, Proc. Natl. Acad. Sci. U. S. A. 116 (2019) 19743–19752. https://doi.org/10.1073/pnas.1900317116.

628 [10] I. Kars, G.H. Krooshof, L. Wagemakers, R. Joosten, J.A.E. Benen, J.A.L. Van Kan,

629 Necrotizing activity of five Botrytis cinerea endopolygalacturonases produced in Pichia

630 pastoris, Plant J. 43 (2005) 213–225. https://doi.org/10.1111/j.1365-

631 313X.2005.02436.x.

632 [11] R.P. Jolie, T. Duvetter, A.M. Van Loey, M.E. Hendrickx, Pectin methylesterase and its

633 proteinaceous inhibitor: A review, Carbohydr. Res. 345 (2010) 2583–2595.

634 https://doi.org/10.1016/j.carres.2010.10.002.

635 [12] R.S. Jayani, S. Saxena, R. Gupta, Microbial pectinolytic enzymes: A review, Process

636 Biochem. 40 (2005) 2931–2944. https://doi.org/10.1016/j.procbio.2005.03.026.

637 [13] H. Suzuki, T. Morishima, A. Handa, H. Tsukagoshi, M. Kato, M. Shimizu,

638 Biochemical Characterization of a Pectate Lyase AnPL9 from Aspergillus nidulans,

639 Appl. Biochem. Biotechnol. (2022). https://doi.org/10.1007/s12010-022-04036-x.

640 [14] G. Limberg, R. Körner, H.C. Buchholt, T.M.I.E. Christensen, P. Roepstorff, J.D.

641 Mikkelsen, Analysis of different de-esterification mechanisms for pectin by enzymatic

642 fingerprinting using endopectin lyase and endopolygalacturonase II from A. Niger,

643 Carbohydr. Res. 327 (2000) 293–307. https://doi.org/10.1016/S0008-6215(00)00067-7.

644 [15] O. Mayans, M. Scott, I. Connerton, T. Gravesen, J. Benen, J. Visser, R. Pickersgill, J.

645 Jenkins, Two crystal structures of pectin lyase A from Aspergillus reveal a pH driven

646 conformational change and striking divergence in the substrate-binding clefts of pectin

647 and pectate lyases, Structure. 5 (1997) 677–689. https://doi.org/10.1016/S0969-

648 2126(97)00222-0.

649 [16] S. Yadav, P.K. Yadav, D. Yadav, K.D.S. Yadav, Pectin lyase: A review, Process

650 Biochem. 44 (2009) 1–10. https://doi.org/10.1016/j.procbio.2008.09.012.

651 [17] F. Sénéchal, C. Wattier, C. Rustérucci, J. Pelloux, Homogalacturonan-modifying

652 enzymes: Structure, expression, and roles in plants, J. Exp. Bot. 65 (2014) 5125–5160.

653 https://doi.org/10.1093/jxb/eru272.

654 [18] B. Zeuner, T.B. Thomsen, M.A. Stringer, K.B.R.M. Krogh, A.S. Meyer, J. Holck,

655 Comparative Characterization of Aspergillus Pectin Lyases by Discriminative

656 Substrate Degradation Profiling, Front. Bioeng. Biotechnol. 8 (2020).

657 https://doi.org/10.3389/fbioe.2020.00873.

658   [19]   G. Yang, W. Chen, H. Tan, K. Li, J. Li, H. Yin, Biochemical characterization and

659   evolutionary analysis of a novel pectate lyase from Aspergillus parasiticus, Int. J. Biol.

660   Macromol. 152 (2020) 180–188. https://doi.org/10.1016/j.ijbiomac.2020.02.279.

661   [20]   M.D. Yoder, S.E. Lietzke, F. Jurnak, Unusual structural features in the parallel β-helix

662   in pectate lyases, Structure. 1 (1993) 241–251. https://doi.org/10.1016/0969-

663   2126(93)90013-7.

664   [21]   J. Vitali, B. Schick, H.C.M. Kester, J. Visser, F. Jurnak, The Three-Dimensional

665   Structure of Aspergillus niger Pectin Lyase B at 1.7-Å Resolution, Plant Physiol. 116

666   (1998) 69–80. https://doi.org/10.1104/pp.116.1.69.

667   [22]   S.E. Lietzke, R.D. Scavetta, M.D. Yoder, F. Jurnak, The Refined Three-Dimensional

668   Structure of Pectate Lyase E from Erwinia chrysanthemi at 2.2 A Resolution, Plant

669   Physiol. 111 (1996) 73–92. https://doi.org/10.1104/pp.111.1.73.

670   [23]   M. Akita, A. Suzuki, T. Kobayashi, S. Ito, T. Yamane, The first structure of pectate

671   lyase belonging to polysaccharide lyase family 3, Acta Crystallogr. Sect. D Biol.

672   Crystallogr. 57 (2001) 1786–1792. https://doi.org/10.1107/S0907444901014482.

673   [24]   R. Pickersgill, J. Jenkins, G. Harris, W. Nasser, J. Robert Baudouy, The structure of

674   Bacillus subtil is pectate lyase in complex with calcium, Nat. Struct. Biol. 1 (1994)

675   717–723. https://doi.org/10.1038/nsb1094-717.

676   [25]   A.S. Luis, J. Briggs, X. Zhang, B. Farnell, D. Ndeh, A. Labourel, A. Baslé, A.

677   Cartmell, N. Terrapon, K. Stott, E.C. Lowe, R. McLean, K. Shearer, J. Schückel, I.

678   Venditto, M.C. Ralet, B. Henrissat, E.C. Martens, S.C. Mosimann, D.W. Abbott, H.J.

679   Gilbert, Dietary pectic glycans are degraded by coordinated enzyme pathways in

680   human colonic Bacteroides, Nat. Microbiol. 3 (2018) 210–219.

681   https://doi.org/10.1038/s41564-017-0079-1.

682   [26]   K. Johansson, M. El-Ahmad, R. Friemann, H. Jörnvall, O. Markovič, H. Eklund,

683   Crystal structure of plant pectin methylesterase, FEBS Lett. 514 (2002) 243–249.

684   https://doi.org/10.1016/S0014-5793(02)02372-4.

685   [27]   S.W. Cho, S. Lee, W. Shin, The X-ray structure of Aspergillus aculeatus

686   Polygalacturonase and a Modeled structure of the Polygalacturonase-Octagalacturonate

687   Complex, J. Mol. Biol. 311 (2001) 863–878. https://doi.org/10.1006/jmbi.2001.4919.

688   [28]   T.N. Petersen, S. Kauppinen, S. Larsen, The crystal structure of rhamnogalacturonase a
689   from Aspergillus aculeatus: A right-handed parallel β helix, Structure. 5 (1997) 533–
690   544. https://doi.org/10.1016/S0969-2126(97)00209-8.

691   [29]   R.D. Scavetta, S.R. Herron, A.T. Hotchkiss, N. Kita, N.T. Keen, J.A.E. Benen, H.C.M.
692   Kester, J. Visser, F. Jurnak, Structure of a plant cell wall fragment complexed to
693   pectate lyase C, Plant Cell. 11 (1999) 1081–1092.
694   https://doi.org/10.1105/tpc.11.6.1081.

695   [30]   A. Blum, M. Bressan, A. Zahid, I. Trinsoutrot-Gattin, A. Driouich, K. Laval,
696   Verticillium Wilt on Fiber Flax: Symptoms and Pathogen Development In Planta, Plant
697   Dis. 102 (2018) 2421–2429. https://doi.org/10.1094/PDIS-01-18-0139-RE.

698   [31]   K. Zeise, A. Von Tiedemann, Host specialization among vegetative compatibility
699   groups of Verticillium dahliae in relation to Verticillium longisporum, J. Phytopathol.
700   150 (2002) 112–119. https://doi.org/10.1046/j.1439-0434.2002.00730.x.

701   [32]   J. Zhang, X. Yu, C. Zhang, Q. Zhang, Y. Sun, H. Zhu, C. Tang, Pectin lyase enhances
702   cotton resistance to Verticillium wilt by inducing cell apoptosis of Verticillium dahliae,
703   J. Hazard. Mater. 404 (2021) 124029. https://doi.org/10.1016/j.jhazmat.2020.124029.

704   [33]   J.Y. Chen, H.L. Xiao, Y.J. Gui, D.D. Zhang, L. Li, Y.M. Bao, X.F. Dai,
705   Characterization of the Verticillium dahliae exoproteome involves in pathogenicity
706   from cotton-containing medium, Front. Microbiol. 7 (2016) 1–15.
707   https://doi.org/10.3389/fmicb.2016.01709.

708   [34]   S.J. Klosterman, Z.K. Atallah, G.E. Vallad, K. V. Subbarao, Diversity, Pathogenicity,
709   and Management of Verticillium Species, Annu. Rev. Phytopathol. 47 (2009) 39–62.
710   https://doi.org/10.1146/annurev-phyto-080508-081748.

711   [35]   Y. Yang, Y. Zhang, B. Li, X. Yang, Y. Dong, D. Qiu, A Verticillium dahliae Pectate
712   Lyase Induces Plant Immune Responses and Contributes to Virulence, Front. Plant Sci.
713   9 (2018) 1–15. https://doi.org/10.3389/fpls.2018.01271.

714   [36]   D. Duressa, A. Anchieta, D. Chen, A. Klimes, M.D. Garcia-Pedrajas, K.F. Dobinson,
715   S.J. Klosterman, RNA-seq analyses of gene expression in the microsclerotia of
716   Verticillium dahliae, BMC Genomics. 14 (2013) 5–18. https://doi.org/10.1186/1471-
717   2164-14-607.

718   [37]   J. Safran, O. Habrylo, M. Cherkaoui, S. Lecomte, A. Voxeur, S. Pilard, S. Bassard, C.
719   Pau-Roblot, D. Mercadante, J. Pelloux, F. Sénéchal, New insights into the specificity
720   and processivity of two novel pectinases from Verticillium dahliae, Int. J. Biol.
721   Macromol. 176 (2021) 165–176. https://doi.org/10.1016/j.ijbiomac.2021.02.035.

722   [38]   A. Lemaire, C. Duran Garzon, A. Perrin, O. Habrylo, P. Trezel, S. Bassard, V.
723   Lefebvre, O. Van Wuytswinkel, A. Guillaume, C. Pau-Roblot, J. Pelloux, Three novel
724   rhamnogalacturonan I- pectins degrading enzymes from Aspergillus aculeatinus:
725   Biochemical characterization and application potential, Carbohydr. Polym. 248 (2020)
726   116752. https://doi.org/10.1016/j.carbpol.2020.116752.

727   [39]   W. Kabsch, Xds., Acta Crystallogr. D. Biol. Crystallogr. 66 (2010) 125–32.
728   https://doi.org/10.1107/S0907444909047337.

729   [40]   W. Kabsch, Integration, scaling, space-group assignment and post-refinement, Acta
730   Crystallogr. Sect. D Biol. Crystallogr. 66 (2010) 133–144.
731   https://doi.org/10.1107/S0907444909047374.

732   [41]   B.W. Matthews, Solvent content of protein crystals., J. Mol. Biol. 33 (1968) 491–497.
733   https://doi.org/10.1016/0022-2836(68)90205-2.

734   [42]   A.J. McCoy, R.W. Grosse-Kunstleve, P.D. Adams, M.D. Winn, L.C. Storoni, R.J.
735   Read, Phaser crystallographic software, J. Appl. Crystallogr. 40 (2007) 658–674.
736   https://doi.org/10.1107/S0021889807021206.

737   [43]   Y. Zheng, C.H. Huang, W. Liu, T.P. Ko, Y. Xue, C. Zhou, R.T. Guo, Y. Ma, Crystal
738   structure and substrate-binding mode of a novel pectate lyase from alkaliphilic Bacillus
739   sp. N16-5, Biochem. Biophys. Res. Commun. 420 (2012) 269–274.
740   https://doi.org/10.1016/j.bbrc.2012.02.148.

741   [44]   D. Liebschner, P. V. Afonine, M.L. Baker, G. Bunkoczi, V.B. Chen, T.I. Croll, B.
742   Hintze, L.W. Hung, S. Jain, A.J. McCoy, N.W. Moriarty, R.D. Oeffner, B.K. Poon,
743   M.G. Prisant, R.J. Read, J.S. Richardson, D.C. Richardson, M.D. Sammito, O. V.
744   Sobolev, D.H. Stockwell, T.C. Terwilliger, A.G. Urzhumtsev, L.L. Videau, C.J.
745   Williams, P.D. Adams, Macromolecular structure determination using X-rays, neutrons
746   and electrons: Recent developments in Phenix, Acta Crystallogr. Sect. D Struct. Biol.
747   75 (2019) 861–877. https://doi.org/10.1107/S2059798319011471.

748   [45]   P. Emsley, B. Lohkamp, W.G. Scott, K. Cowtan, Features and development of Coot,

749   Acta Crystallogr. Sect. D Biol. Crystallogr. 66 (2010) 486–501.

750   https://doi.org/10.1107/S0907444910007493.

751   [46] L. Hocq, S. Guinand, O. Habrylo, A. Voxeur, W. Tabi, J. Safran, F. Fournet, J.-M.

752   Domon, J.-C. Mollet, S. Pilard, C. Pau- Roblot, A. Lehner, J. Pelloux, V. Lefebvre,

753   The exogenous application of AtPGLR, an endo - polygalacturonase, triggers pollen

754   tube burst and repair, Plant J. 103 (2020) 617–633. https://doi.org/10.1111/tpj.14753.

755   [47] K. Lindorff-Larsen, S. Piana, K. Palmo, P. Maragakis, J.L. Klepeis, R.O. Dror, D.E.

756   Shaw, Improved side-chain torsion potentials for the Amber ff99SB protein force field,

757   Proteins Struct. Funct. Bioinforma. 78 (2010) 1950–1958.

758   https://doi.org/10.1002/prot.22711.

759   [48] W.L. Jorgensen, J. Chandrasekhar, J.D. Madura, R.W. Impey, M.L. Klein, Comparison

760   of simple potential functions for simulating liquid water, J. Chem. Phys. 79 (1983)

761   926–935. https://doi.org/10.1063/1.445869.

762   [49] J.S. Rowlinson, The Maxwell-boltzmann distribution, Mol. Phys. 103 (2005) 2821–

763   2828. https://doi.org/10.1080/002068970500044749.

764   [50] H.J.C. Berendsen, J.P.M. Postma, W.F. Van Gunsteren, A. Dinola, J.R. Haak,

765   Molecular dynamics with coupling to an external bath, J. Chem. Phys. 81 (1984) 3684–

766   3690. https://doi.org/10.1063/1.448118.

767   [51] M. Parrinello, A. Rahman, Polymorphic transitions in single crystals: A new molecular

768   dynamics method, J. Appl. Phys. 52 (1981) 7182–7190.

769   https://doi.org/10.1063/1.328693.

770   [52] T. Darden, D. York, L. Pedersen, Particle mesh Ewald: An N·log(N) method for Ewald

771   sums in large systems, J. Chem. Phys. 98 (1993) 10089–10092.

772   https://doi.org/10.1063/1.464397.

773   [53] T. Kluyver, B. Ragan-Kelley, F. Pérez, B. Granger, M. Bussonnier, J. Frederic, K.

774   Kelley, J. Hamrick, J. Grout, S. Corlay, P. Ivanov, D. Avila, S. Abdalla, C. Willing,

775   Jupyter Notebooks—a publishing format for reproducible computational workflows,

776   Position. Power Acad. Publ. Play. Agents Agendas - Proc. 20th Int. Conf. Electron.

777   Publ. ELPUB 2016. (2016) 87–90. https://doi.org/10.3233/978-1-61499-649-1-87.

778   [54] J.D. Hunter, Matplotlib: A 2D graphics environment, Comput. Sci. Eng. 9 (2007) 90–

779   95. https://doi.org/10.1109/MCSE.2007.55.

780   [55] W. Humphrey, A. Dalke, K. Schulten, VMD: Visual Molecular Dynamics, J. Mol.
781   Graph. 14 (1996) 33–38.

782   [56] S.J. Klosterman, K. V. Subbarao, S. Kang, P. Veronese, S.E. Gold, B.P.H.J. Thomma,
783   Z. Chen, B. Henrissat, Y.-H. Lee, J. Park, M.D. Garcia-Pedrajas, D.J. Barbara, A.
784   Anchieta, R. de Jonge, P. Santhanam, K. Maruthachalam, Z. Atallah, S.G. Amyotte, Z.
785   Paz, P. Inderbitzin, R.J. Hayes, D.I. Heiman, S. Young, Q. Zeng, R. Engels, J. Galagan,
786   C.A. Cuomo, K.F. Dobinson, L.-J. Ma, Comparative Genomics Yields Insights into
787   Niche Adaptation of Plant Vascular Wilt Pathogens, PLoS Pathog. 7 (2011) e1002137.
788   https://doi.org/10.1371/journal.ppat.1002137.

789   [57] S. Mandelc, B. Javornik, The secretome of vascular wilt pathogen Verticillium albo-
790   atrum in simulated xylem fluid, Proteomics. 15 (2015) 787–797.
791   https://doi.org/10.1002/pmic.201400181.

792   [58] S.D. Liston, S.A. McMahon, A. Le Bas, M.D.L. Suits, J.H. Naismith, C. Whitfield,
793   Periplasmic depolymerase provides insight into ABC transporter-dependent secretion
794   of bacterial capsular polysaccharides, Proc. Natl. Acad. Sci. U. S. A. 115 (2018)
795   E4870–E4879. https://doi.org/10.1073/pnas.1801336115.

796   [59] J. Jenkins, R. Pickersgill, The architecture of parallel β-helices and related folds, Prog.
797   Biophys. Mol. Biol. 77 (2001) 111–175. https://doi.org/10.1016/S0079-
798   6107(01)00013-X.

799   [60] M.D. Yoder, F. Jurnak, The Refined Three-Dimensional Structure of Pectate Lyase C
800   lmplications for an Enzymatic Mechanism, Plant Physiol. 107 (1995) 349–364.

801   [61] Y. van Santen, J.A.E. Benen, K.H. Schroter, K.H. Kalk, S. Armand, J. Visser, B.W.
802   Dijkstra, 1.68-angstrom crystal structure of endopolygalacturonase II from Aspergillus
803   niger and identification of active site residues by site-directed mutagenesis, J. Biol.
804   Chem. 274 (1999) 30474–30480. https://doi.org/10.1074/JBC.274.43.30474.

805   [62] S.E. Lietzke, R.D. Scavetta, M.D. Yoder, The Refined Three-Dimensional Structure of
806   Pectate Lyase E from, Plant Physiol. 111 (1996) 73–92.

807   [63] B. Henrissat, S.E. Heffron, M.D. Yoder, S.E. Lietzke, F. Jurnak, Functional
808   implications of structure-based sequence alignment of proteins in the extracellular

809   pectate lyase superfamily., Plant Physiol. 107 (1995) 963–76.

810   https://doi.org/10.1104/pp.107.3.963.

811 [64] N. Kita, C.M. Boyd, M.R. Garrett, F. Jurnak, N.T. Keen, Differential Effect of Site-

812   directed Mutations in pelC on Pectate Lyase Activity, Plant Tissue Maceration, and

813   Elicitor Activity, J. Biol. Chem. 271 (1996) 26529–26535.

814   https://doi.org/10.1074/jbc.271.43.26529.

815 [65] S. Ali, C.R. Søndergaard, S. Teixeira, R.W. Pickersgill, Structural insights into the loss

816   of catalytic competence in pectate lyase activity at low pH, FEBS Lett. 589 (2015)

817   3242–3246. https://doi.org/10.1016/j.febslet.2015.09.014.

818 [66] C. Creze, S. Castang, E. Derivery, R. Haser, N. Hugouvieux-Cotte-Pattat, V.E.

819   Shevchik, P. Gouet, The Crystal Structure of Pectate Lyase PelI from Soft Rot

820   Pathogen *Erwinia chrysanthemi* in Complex with Its Substrate, J. Biol. Chem. 283

821   (2008) 18260–18268. https://doi.org/10.1074/jbc.M709931200.

822 [67] A. Dubey, S. Yadav, M. Kumar, G. Anand, D. Yadav, Molecular Biology of Microbial

823   Pectate Lyase: A Review, Br. Biotechnol. J. 13 (2016) 1–26.

824   https://doi.org/10.9734/bbj/2016/24893.

825 [68] H.G. Ouattara, S. Reverchon, S.L. Niamke, W. Nasser, Biochemical Properties of

826   Pectate Lyases Produced by Three Different Bacillus Strains Isolated from Fermenting

827   Cocoa Beans and Characterization of Their Cloned Genes, Appl. Environ. Microbiol.

828   76 (2010) 5214–5220. https://doi.org/10.1128/AEM.00705-10.

829 [69] M. Soriano, A. Blanco, P. Díaz, F.I.J. Pastor, An unusual pectate lyase from a Bacillus

830   sp. with high activity on pectin: Cloning and characterization, Microbiology. 146

831   (2000) 89–95. https://doi.org/10.1099/00221287-146-1-89.

832 [70] G. Chilosi, P. Magro, Pectin lyase and polygalacturonase isoenzyme production by

833   Botrytis cinerea during the early stages of infection on different host plants, J. Plant

834   Pathol. 79 (1997) 61–69. https://doi.org/10.1080/01904167.2015.1112950.

835 [71] S. Hassan, V.E. Shevchik, X. Robert, N. Hugouvieux-Cotte-Pattat, PelN is a new

836   pectate lyase of dickeya dadantii with unusual characteristics, J. Bacteriol. 195 (2013)

837   2197–2206. https://doi.org/10.1128/JB.02118-12.

838 [72] C. Zhou, Y. Xue, Y. Ma, Cloning, evaluation, and high-level expression of a thermo-

839   alkaline pectate lyase from alkaliphilic Bacillus clausii with potential in ramie

840   degumming, Appl. Microbiol. Biotechnol. 101 (2017) 3663–3676.

841   https://doi.org/10.1007/s00253-017-8110-2.

842   [73] W. Sukhumsiirchart, S. Kawanishi, W. Deesukon, K. Chansiri, H. Kawasaki, T.

843   Sakamoto, Purification, Characterization, and Overexpression of Thermophilic Pectate

844   Lyase of Bacillus sp. RN1 Isolated from a Hot Spring in Thailand, Biosci. Biotechnol.

845   Biochem. 73 (2009) 268–273. https://doi.org/10.1271/bbb.80287.

846   [74] C. Zhang, J. Yao, C. Zhou, L. Mao, G. Zhang, Y. Ma, The alkaline pectate lyase

847   PEL168 of Bacillus subtilis heterologously expressed in Pichia pastorisis more stable

848   and efficient for degumming ramie fiber, BMC Biotechnol. 13 (2013) 26.

849   https://doi.org/10.1186/1472-6750-13-26.

850   [75] P. Yuan, K. Meng, Y. Wang, H. Luo, P. Shi, H. Huang, T. Tu, P. Yang, B. Yao, A

851   Low-Temperature-Active Alkaline Pectate Lyase from Xanthomonas campestris

852   ACCC 10048 with High Activity over a Wide pH Range, Appl. Biochem. Biotechnol.

853   168 (2012) 1489–1500. https://doi.org/10.1007/s12010-012-9872-8.

854   [76] Y. Tang, P. Wu, S. Jiang, J.N. Selvaraj, S. Yang, G. Zhang, A new cold-active and

855   alkaline pectate lyase from Antarctic bacterium with high catalytic efficiency, Appl.

856   Microbiol. Biotechnol. 103 (2019) 5231–5241. https://doi.org/10.1007/s00253-019-

857   09803-1.

858   [77] P. Wu, S. Yang, Z. Zhan, G. Zhang, Origins and features of pectate lyases and their

859   applications in industry, Appl. Microbiol. Biotechnol. 104 (2020) 7247–7260.

860   https://doi.org/10.1007/s00253-020-10769-8.

861   [78] Z. Zhou, Y. Liu, Z. Chang, H. Wang, A. Leier, T.T. Marquez-Lago, Y. Ma, J. Li, J.

862   Song, Structure-based engineering of a pectate lyase with improved specific activity for

863   ramie degumming, Appl. Microbiol. Biotechnol. 101 (2017) 2919–2929.

864   https://doi.org/10.1007/s00253-016-7994-6.

865   [79] M.D. Joshi, G. Sidhu, I. Pot, G.D. Brayer, S.G. Withers, L.P. McIntosh, Hydrogen

866   bonding and catalysis: A novel explanation for how a single amino acid substitution

867   can change the pH optimum of a glycosidase, J. Mol. Biol. 299 (2000) 255–279.

868   https://doi.org/10.1006/jmbi.2000.3722.

869   [80] T. Yasuda, H. Takeshita, R. Iida, M. Ueki, T. Nakajima, Y. Kaneko, K. Mogi, Y.

Kominato, K. Kishi, A single amino acid substitution can shift the optimum pH of DNase I for enzyme activity: Biochemical and molecular analysis of the piscine DNase I family, Biochim. Biophys. Acta - Gen. Subj. 1672 (2004) 174–183. https://doi.org/10.1016/j.bbagen.2004.03.012.

[81] H. Shibuya, S. Kaneko, K. Hayashi, A single amino acid substitution enhances the catalytic activity of family 11 xylanase at alkaline pH, Biosci. Biotechnol. Biochem. 69 (2005) 1492–1497. https://doi.org/10.1271/bbb.69.1492.

[82] M. Goetz, T. Roitsch, The different pH optima and substrate specificities of extracellular and vacuolar invertases from plants are determined by a single amino-acid substitution, Plant J. 20 (1999) 707–711. https://doi.org/10.1046/j.1365-313X.1999.00628.x.